

gradual increase up to 15 ns and seems to be almost constant after 20 ns. Plots of rmsd in Figure S1 were obtained from the coordinates of main chain atoms of the whole HA. The N-terminal domain of the HA1 subunit is so flexible that rmsd values are considerably large. Hence, rmsd values were calculated again with respect to the main chain atoms of only the HA2 subunit with excluding the C-terminal region, aa 176–222. The rmsd curves only for HA2 in Supplementary Figure S2 also became constant after 20 ns for every model. Accordingly, protein conformations for the respective models were judged to be equilibrated.

Principal component analysis (PCA) in Supplementary Figure S3 indicates that the trajectory structures for the last 5 ns are in a single conformation for every model. The equilibration of the simulation is also confirmed from these PCA plots. In order to extract the plausible protein structure, the averaged structure was obtained using 500 trajectory structures from the last 5 ns of MD simulation. The rmsd between each trajectory structure and the average structure was calculated, and then one trajectory structure with the smallest rmsd value was determined to be the plausible protein structure. At a glance, there is no prominent difference among the 4 models in terms of shape of the trimer, conformation of the HA1 and HA2 subunits, or position of helices. Although no significant apparent change is seen in the backbone of HA, there appears a notable difference in the location of side chains. The differences in the side chain will be responsible for the change in binding affinity and inhibitory activity of inhibitors.

**Binding of an Inhibitor to HA.** By means of docking simulation, an inhibitor, stachyflin, was bound to the HAs, using the respective plausible protein structures obtained by MD calculations. In the wild-type HA, stachyflin was bound near Asp109 of the HA2 subunit (Figure 2). Hydrophobic interactions were observed between the B ring of stachyflin and Phe37 of HA1, between the C ring of stachyflin and Phe110 of HA2, and between the D ring and Leu113. Hydrogen bonds were formed between the O atom on the D ring of stachyflin and the amino group of Asn114 in HA2 and between the O atom on the E ring and the amino group of Asn117.

In mutant 2, stachyflin was bound to a location similar to that of the wild-type (Supplementary Figure S4c), while the docking simulation showed binding of stachyflin at the central space among three helices of the HA2 trimer in mutants 1 and 3 (Figures S4b and d). Judging from the binding affinity evaluated by ASP score function (Supplementary Table S2), the binding of stachyflin to the wild-type HA is the most stable. All of the mutants showed notable decrease in binding affinity compared to that of the wild-type.

An amino acid mutation of K51R in HA2 commonly appeared in the three mutants, suggesting that K51R was the primary mutation for drug resistance. Other mutations, K121E and V176I, will enhance the resistance. All of these amino mutations are, however, distant from the stachyflin binding site. Our MD simulation clearly indicated that inner helices of HA2 subunit were rotated (Figure 3a). One of the three inner helices, chain D in nomenclature in PDB 1RD8, was rotated by 10.8° in mutant 1 and by 15.0° in mutant 2 compared to the wild-type (Figure 3b). The amino group on the side chain of Lys51 makes a strong hydrogen bond with the hydroxy group of Thr107 of HA2 (Figure 3c). Arg is also a positively charged amino acid residue, but the length of the side chain is longer than that of Lys. When Lys is converted into Arg, the side chain

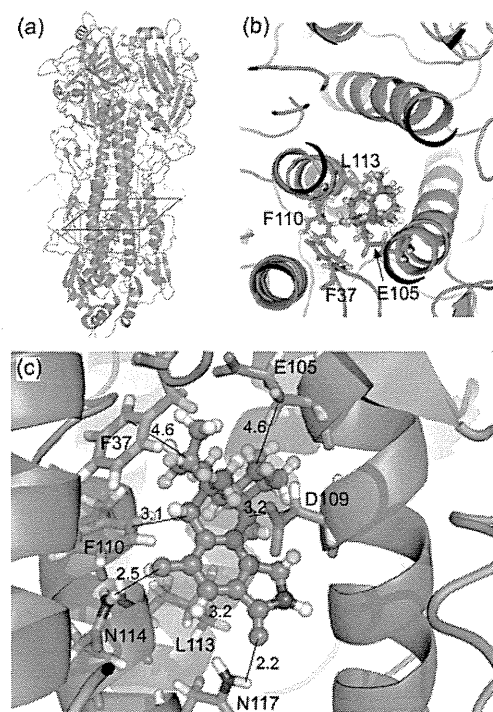


**Figure 2.** (a) Complex structure of stachyflin and hemagglutinin obtained by the ligand docking simulation. (b) Binding site of stachyflin viewed in a plane perpendicular to the helices of the HA2 subunit. (c) Binding mode of stachyflin, shown in a magnified view of the area indicated by a red frame in panel a. Stachyflin is bound to the space between two helices of HA2 subunit, making strong interaction with side chains of Asp109, Phe110, and Leu113. The interaction distances are in Å.

of the residue at codon 51 expands and pushes T107. The side chain of Thr107 serves as a lever to rotate the helix. The position of the side chain of Asp109 is largely deviated from that of the wild-type because of the closeness to Thr107. Lys121 has a strong interaction with the carboxy group of Asp18 of the HA1 subunit. When Lys is converted into Glu in the K121E mutation, the side chain of Glu121 and Asp18 of HA1 causes repulsion to increase the distance between them. This repulsion assists the helix rotation, and the deviation of Leu113 and Asn114 from the wild-type will be enhanced because of the closeness to Glu121. To monitor the helix rotation, the angle between the line connecting the  $C\alpha$  and  $C\beta$  atoms of Asp109 on the inner helix chain D and the line connecting the Asp109  $C\alpha$  atom on chain D and the Phe110  $C\alpha$  atom on another inner helix chain B was measured through the simulation as shown in Supplementary Figure S5. A significant angle change was observed after 10 ns for every model. The distances between the  $N\zeta$  atom of Lys51 (or  $C\zeta$  in K51R) of HA2 and the  $O\gamma$  atom of Thr107 of HA2 and also between the  $N\zeta$  atom of Lys121 (or  $C\delta$  in K121E) of HA2 and  $C\gamma$  of Asp18 of HA1 were monitored as shown in Supplementary Figure S6. Because HA is a trimer and there exist three HA1 and three HA2 subunits in the calculation models, three combinations of those interatomic distances were measured through the simulation. The distance plots in Figure S6 indicate that the interaction between the residues at codon 51 and codon 107 is quite stable in the wild-type HA. In contrast, some of these distances occasionally increased in the mutants. The distance between the residues at codon 121 of HA2 and at codon 18 of HA1 ceaselessly fluctuated in all

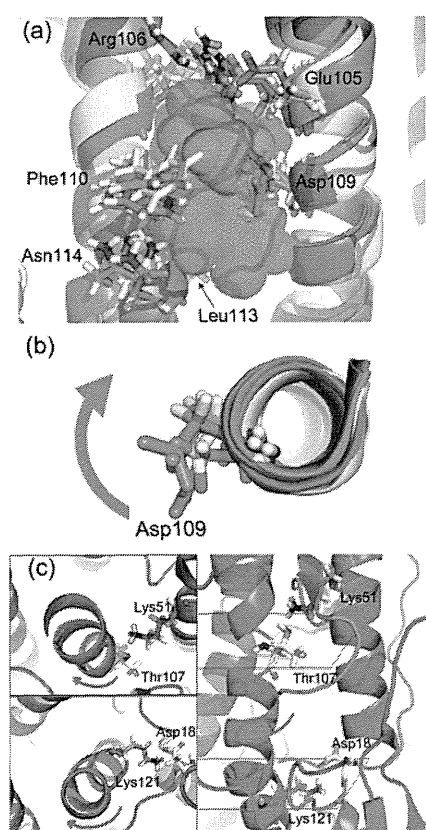


**Figure 3.** (a) Superposition of the hemagglutinin structures of mutants on that of the wild-type. The wild type is colored green and mutants 1, 2, and 3 are colored cyan, magenta, yellow, respectively. The binding area of stachyflin to the wild-type HA is shown in a mesh representation. There is no significant change in positions of helices. However, the amino acid mutations cause rotation of helices. The rotation angle is estimated from the position of C $\beta$  atom of Asp109, as shown in panel b. Thr107 in HA2 subunit and Asp18 in HA1 subunit are deeply involved in the helix rotation induced by K51R and K121E mutations, respectively, as shown in panel c. Two illustrations on the left side are depicted around the planes perpendicular to the helices and containing Thr107 or Lys121, respectively. The planes are indicated by blue and red frames in the right side illustration in panel c.

models. A strong interaction was, however, established at least for one combination of Lys121 and Asp18 in the wild-type.

The helix rotation pointed out above is the reason for the decrease in inhibitory activity of stachyflin to the resistant mutants. In the mutants, the side chains of Asp109 and Leu113 are displaced and occupy the space that stachyflin was bound to in the wild-type HA. The side chains of Phe110 and Asn114 are also displaced and move away from the stachyflin binding site as shown in Supplementary Figure S7. Therefore, stachyflin would not be bound to HA stably any more. The helix rotation in mutant 3 is small. This is naturally understood because the influence of V176I mutation in the HA1 subunit is slight. This finding suggests that some degree of flexibility is favorable to HA inhibitors for releasing the strain due to the helix rotation. Therefore, compounds bearing a complicated heteroring structure are disadvantageous. Instead, a single bond connection of separated ring domains can be a good chemical frame to maintain structural flexibility.

Conformational change accompanying helix rotation has been reported for other kinds of transmembrane proteins. For example, an X-ray crystallographic analysis of the human  $\beta$ 2

adrenergic G-protein-coupled receptor<sup>14</sup> suggested that a rotational motion was observed for one of the transmembrane helices owing to the binding of a ligand for the receptor. An electron paramagnetic resonance measurement<sup>15</sup> and a computational analysis<sup>16</sup> indicated that light adsorption induced a conformational change of retinal chromophore in sensory rhodopsin and this conformational change caused the rotation of transmembrane helix TM1 to lead signal transduction of the sensory protein.

**Search for Active Compounds.** The natural product stachyflin possesses a unique pentacyclo structure in which each ring is labeled as A, B, C, D, and E, respectively. Rings AB are composed of a naphthol skeleton, and rings DE are composed of an indol frame. Ring C bears a pyran structure and connects rings AB and rings DE. Rings ABC are fused in *cis*-form, and the oxygen of pyran is bonded to the carbon at the junction of rings AB. Furthermore, stachyflin contains 5 chiral centers, in which all of the chiral carbons are located on rings AB. Therefore, the naphthol moiety and its connection to pyran make the chemical structure of stachyflin highly complicated. A hydroxy group and carbonyl oxygen are bound to the indol ring, which characterizes the electrostatic property of stachyflin. The hydroxy group of naphthol is another factor to characterize the polar feature of this natural product.

Eight chemical compounds were selected by an *in silico* screening using the pharmacophore of stachyflin (Table 1). All of the selected compounds were produced by organic synthesis and are available by purchase. The molecular weights of these compounds range from 304 to 341. Compound 1 bears two ester bonds and a benzofuran moiety corresponding to rings C and D of stachyflin in superimposition. Compound 2 bears a thieno-pyrimidine, which corresponds to rings D and E of stachyflin and a phenyl-cyclopentane corresponding to rings A and B. Two benzene rings are connected *via* a dichloromethyl-carbonyl group in compound 3. Methylbenzoic acid methyl-ester in compound 4 corresponds to rings D and E, and dimethyl-diazolane is connected by a sulfonyloxy group. Thieno-pyrimidine in compound 5 corresponds to rings D and E, and another thiophene corresponds to ring A. The molecular weight of compound 6 is the largest among the selected compounds, and methylester-benzene corresponds to rings D and E and pyridyl-triazole corresponds to rings A and B. Compound 7 bears a seven-membered ring containing two nitrogen atoms. Hydroxybenzene in compound 8 corresponds to ring B of stachyflin.

**Assay for Antiviral Activity.** The 8 selected compounds were tested in an influenza virus cell culture assay (Table 1). Compounds 4 and 5 were found to have significant antiviral activity ( $EC_{50} < 5 \mu M$ ). Although compound 2 was the most highly potent with an  $EC_{50}$  of  $3 \mu M$ , compound 2 exhibited significant cytotoxicity at a concentration of  $6 \mu M$ , measured by an MTT assay with MDCK cells. Since compounds 4 and 5 showed no noticeable cytotoxicity, these two compounds were chosen as the structural core in the next step for organic synthesis.

The binding modes of compounds 4 and 5 to the wild-type HA were predicted by performing docking simulation. The most probable docking structures are shown in Figure 4a and b, which were determined from the score ranking for 50 docking poses. The two compounds are bound to almost the same position as stachyflin is. That is, these compounds are located not in the central space of HA2 trimer but at a position in the middle of two helices of the HA2 subunit. The calculated

Table 1. Structures and Inhibitory Activities of the Chemical Compounds Obtained through an *in Silico* Screening

| Compound | Structure | Superimposition <sup>a)</sup> | EC <sub>50</sub> (μM) | CC <sub>50</sub> (μM) |
|----------|-----------|-------------------------------|-----------------------|-----------------------|
| 1        |           |                               | 9.0                   | > 60                  |
| 2        |           |                               | 3.0 >                 | 5.9                   |
| 3        |           |                               | > 32                  | > 60                  |
| 4        |           |                               | 4.4                   | > 60                  |
| 5        |           |                               | 4.9                   | > 60                  |
| 6        |           |                               | 17.9                  | > 60                  |
| 7        |           |                               | 31.4                  | > 60                  |
| 8        |           |                               | 14.9                  | > 60                  |

<sup>a</sup>Stachyflin is depicted in green stick representation, while compounds are blue.

binding affinities of these two compounds in ASP score are lower than that of stachyflin (TSupplementary able S2) but higher than that in the cases of stachyflin bound to the three kinds of mutants.

**Synthesis of Analogue Compounds.** Compound 4 bears a structural core of vanillic acid. Based on the vanillic acid methylester core, 22 derivatives from compound 4 were synthesized as shown in Table 2, where the functional group at the fourth position of the benzoic acid was modulated. A highly potent compound (9) was found in the analogues in which methylsulfonyl was connected to the fourth position. The incorporation of benzyl or methylphenyl (10, 12) showed no inhibitory activity, while moderate activity was observed in case of phenyl only (11). This means that a small chemical group is favorable for the substitute connecting *via* the sulfonyloxy group. Conversion of the sulfonyl group into an ester bond (13–15) resulted in complete loss of compound potency, regardless of the size of the substitutes connected to

the ester. Substitution of the sulfonyl group by an alkyl chain (16–20) resulted in loss of inhibitory activity. Only compound 18 in which the sulfonyl group was substituted by benzyl showed slight inhibitory activity. Then the effect of addition of functional groups to the benzyl (21–28) was surveyed. Compound 22 containing an oxybenzyl group at the *para*-position of the benzyl exhibited high compound potency. The inhibitory activity was maintained with the addition of methoxy or trifluoromethyl at the *para*-position, while the incorporation of other kinds of functional groups (23–25) or the addition of trifluoromethyl at the *ortho*- or *meta*-position (27, 28) resulted in loss of inhibitory activity. Conversion of the sulfonyloxy group into an amino group (29, 30) was tested. None of the derivatives showed noticeable increase in compound potency.

Compound 5 bears a heteroring core of thieno-pyrimidine, and a dimethyl-aminy-thienyl group is connected to the heteroring *via* amine. Keeping the heteroring core, 9 derivatives from compound 5 were synthesized as shown in Table 3. The

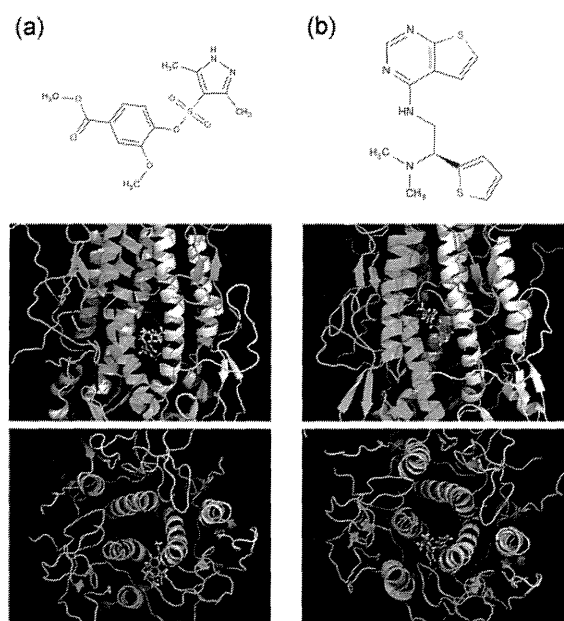


**Figure 4.** Hit chemicals found through *in silico* screening: (a) compound 4 and (b) compound 5. Top: chemical structure. Middle: binding site of the compound predicted by the docking simulation. Bottom: binding position of the compound viewed from the direction of subunit HA1.

introduction of benzyl *via* amine group (**31**) resulted in an increase in inhibitory activity. In contrast, conversion into dimethylamine (**32**, **33**) resulted in loss of compound potency. Interestingly, while conversion into methyl-piperazine (**34**) resulted in a decrease in inhibitory activity, its hydrochloride salt (**35**) exhibited a high compound potency. Phenyl-piperazine (**36**) also exhibited a considerably high inhibitory activity. The conversion of thiophene of compound **5** into benzene (**37**) exhibited a high compound potency, while its chiral analogue (**38**) showed no inhibitory activity. This chiral-selective compound potency was confirmed by substitution of a Boc protection group (**39**) for the dimethylamine of compound **37**.

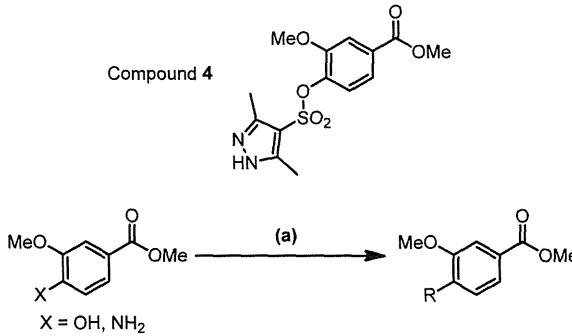
**Actions of Active Compounds for Blocking HA.** Fusion of the membrane is an essential process in the entry of influenza virus into the host cell. HA mediates this process through two functions in the early stage of the viral life cycle.<sup>17</sup> One is anchoring at sialylated glycoprotein receptors on the cell membrane surface. The other is the low-pH induced conformational change that initiates the exposure of a fusion peptide, a hydrophobic N-terminal segment buried in the HA trimer interface, to be inserted into the endosomal membrane. Stachyflin is assumed to block this fusogenic process of HA.<sup>12,13</sup> Indeed, in the predicted binding structure shown in Figure 2, stachyflin is combined with HA with the formation of two strong hydrogen bonds and three strong aromatic ring-involved hydrophobic interactions.

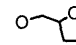
Several other compounds blocking the fusogenic activity of HA have been identified.<sup>18–22</sup> An active compound<sup>18</sup> bears a naphthoquinone skeleton, which is commonly seen in stachyflin as rings AB. Another compound<sup>19</sup> contains a quinolizin moiety connected to a benzamide skeleton, and a one-step virus growth experiment indicated that this compound mainly inhibited virus proliferation at the early stage of the replication cycle. Therefore, a quinoline skeleton is one of the effective chemical cores for binding to HA. A compound

containing piperidine connected to trifluoro-methylbenzoyl also showed high inhibitory activity for influenza virus replication.<sup>20</sup> Ligand docking calculation suggested that this compound was bound to a site near Phe110 of the HA2 subunit, which is almost identical to the binding site of stachyflin obtained in this work as shown in Figure 2. A compound analogue to podocarpic acid was identified as an inhibitor of type A viruses<sup>21</sup> and showed a high inhibitory activity especially for Kawasaki strain but was not so sensitive to WSN strain. In contrast, some recently identified blockers are targeted at another domain of HA.<sup>23,24</sup> Some peptides mimicking sialic acid were shown to inhibit the entry of viruses into host cells, attached to the receptor-binding site of HA.<sup>23</sup> Synthesized macromolecules containing three sialyllactoses linked with trisphenol or trisaniline were reported to inhibit viral replication, combined with the receptor-binding site of HA.<sup>24</sup> Recently, an HA inhibitor bearing a benzenesulfonamide core was identified through structural modifications of a salicylamide derivative.<sup>25</sup> It is interesting to note that the chemical structure of this agent resembles that of compound **9** in Table 2 to some extent.

In most of the active compounds, susceptibility varies among strains of influenza viruses and the inhibitory activity is drastically decreased due to the acquirement of resistant mutation. Our MD simulation demonstrated that the rotation of helices is the reason for the reduction of compound potency. Due to the increase in performance of computers and the development of calculation methodology, several computational analyses have recently been carried out.<sup>26–32</sup> Quantum mechanical calculations using the fragment molecular orbital method were used to investigate the role of key amino acid residues in recognizing sialoglycoproteins on the host cell surface<sup>26</sup> or in combining with neutralizing monoclonal antibodies.<sup>27</sup> Huge MD simulations were performed to examine the interaction between HA and sialoglycans<sup>28</sup> and clarify the reason for mutations at the receptor-recognizing site.<sup>29</sup> MD simulations were also employed to evaluate the binding free energy<sup>30</sup> and to interpret the difference in receptor specificity.<sup>31</sup> A computational approach was further demonstrated to be quite helpful for designing protein peptides that strongly inhibit the function of HA.<sup>32</sup>

**Pharmaceutical Properties of Hit Chemicals.** Since stachyflin exhibits a highly potent anti-influenza activity for the wild-type WSN strain and is a challenging synthetic target due to its unique alkaloid structure, two research groups have so far attempted total synthesis of stachyflin. The first total synthesis of racemic ( $\pm$ )-stachyflin was reported by Taishi *et al.*,<sup>11</sup> in which the characteristic structure of 5 heterorings was built one by one in 29 steps. The first enantioselective total synthesis of (+)-stachyflin was recently achieved by Watanabe *et al.*,<sup>33</sup> utilizing an acid-induced domino epoxide-opening, rearrangement, cyclization reaction.<sup>34</sup> These synthetic studies suggest the possibility for producing stachyflin analogues and encourage the development of stachyflin-based antiviral agents. The complexity in synthesis is, however, disadvantageous from the viewpoint of productivity in manufacturing. Carey and co-workers analyzed the reactions used for the preparation of drug candidate molecules,<sup>35</sup> surveying 128 compounds produced in the departments of process chemistry of three major pharmaceutical companies. According to their analysis, the average number of chemical steps for synthesizing one candidate is 8.1. Compounds containing a chiral center account for about half of the 128 molecules. Therefore, the structural

Table 2. Structures and Inhibitory Activities of the Synthesized Analogues to Compound 4, Which Bears a Vanillic Acid Core<sup>a</sup>


| Compound | X               | R   | Temp. (°C) | Time (h) | Yield (%) | EC <sub>50</sub> (μM) |
|----------|-----------------|---|------------|----------|-----------|-----------------------|
| 9        |                 | OSO <sub>2</sub> Me   | rt         | 3        | 71        | 0.9                   |
| 10       | OH              | OSO <sub>2</sub> CH <sub>2</sub> Ph   | rt         | 3        | 75        | >10                   |
| 11       |                 | OSO <sub>2</sub> Ph   | rt         | 6        | 81        | 7.0                   |
| 12       |                 | OSO <sub>2</sub> <i>p</i> -MeC <sub>6</sub> H <sub>4</sub>                        | rt         | 6        | 82        | >10                   |
| 13       |                 | OCOMe   | rt         | 3        | 35        | >10                   |
| 14       | OH              | OCOCH <sub>2</sub> Cl   | rt         | 3        | 66        | >10                   |
| 15       |                 | OCOPh   | reflux     | 3        | 80        | >10                   |
| 16       |                 |  | reflux     | 24       | 93        | >10                   |
| 17       | OH              | OCH <sub>2</sub> <i>t</i> -Bu   | reflux     | 72       | 21        | >10                   |
| 18       |                 | OCH <sub>2</sub> Ph   | rt         | 8        | 81        | 8.3                   |
| 19       |                 | OCH <sub>2</sub> CH <sub>2</sub> Ph   | reflux     | 24       | 70        | >10                   |
| 20       |                 | OCH <sub>2</sub> (CH <sub>2</sub> ) <sub>2</sub> Ph                               | reflux     | 24       | 91        | >10                   |
| 21       |                 | OCH <sub>2</sub> <i>p</i> -MeOC <sub>6</sub> H <sub>4</sub>                       | rt         | 12       | 72        | 8.1                   |
| 22       |                 | OCH <sub>2</sub> <i>p</i> -BnOC <sub>6</sub> H <sub>4</sub>                       | rt         | 12       | 83        | 2.5                   |
| 23       |                 | OCH <sub>2</sub> <i>p</i> -NO <sub>2</sub> C <sub>6</sub> H <sub>4</sub>          | rt         | 12       | 67        | >10                   |
| 24       |                 | OCH <sub>2</sub> <i>p</i> -FC <sub>6</sub> H <sub>4</sub>                         | rt         | 12       | 88        | >10                   |
| 25       | OH              | OCH <sub>2</sub> 2,3,4,5,6-F <sub>5</sub> C <sub>6</sub>                          | rt         | 12       | 82        | >10                   |
| 26       |                 | OCH <sub>2</sub> <i>p</i> -CF <sub>3</sub> C <sub>6</sub> H <sub>4</sub>          | rt         | 12       | 79        | 8.2                   |
| 27       |                 | OCH <sub>2</sub> <i>o</i> -CF <sub>3</sub> C <sub>6</sub> H <sub>4</sub>          | rt         | 12       | 76        | >10                   |
| 28       |                 | OCH <sub>2</sub> <i>m</i> -CF <sub>3</sub> C <sub>6</sub> H <sub>4</sub>          | rt         | 12       | 68        | >10                   |
| 29       |                 | NHCH <sub>2</sub> Ph  |            |          | 54        | 8.5                   |
| 30       | NH <sub>2</sub> | N(CH <sub>2</sub> Ph) <sub>2</sub>  | rt         | 12       | 27        | >10                   |

<sup>a</sup>Condition: (a) K<sub>2</sub>CO<sub>3</sub>, R-Cl, CH<sub>3</sub>CN, temp, time, 21–93%.

core of stachyflin would not be suitable for scale-up synthesis in terms of the number of synthetic steps and the number of chiral centers. In this study, we provided two scaffolds exhibiting antiviral activity. Most of the compounds shown in Tables 2 and 3 were synthesized within 3 steps, except for compounds 37–39. Compounds 37–39 include chiral centers, and the synthesis of these compounds was achieved at most within 8 steps. Accordingly, the proposed scaffolds are feasible for diverse modulation of functional groups and then ones of the chemical bases for the development of HA inhibitors.

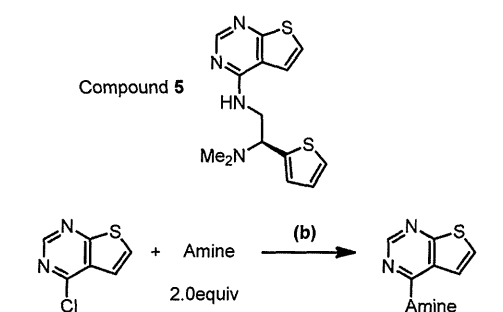
A requirement of antiviral drugs in clinical use is inhibitory activity for a broad range of viral strains. We tested the potency of several compounds synthesized in this study using A/Vietnam/1194/2004 (H5N1) strain,<sup>36</sup> which causes severe pathological conditions for humans and is one of the viruses attracting keen concern for the threat of a pandemic. A cell-based antiviral assay indicated that compounds 31 and 39 were effective for this H5N1 type virus with IC<sub>50</sub> values of 0.2 and 5.2 μM, respectively. This suggests that the scaffolds found in this study will maintain compound potency over different types of influenza viruses.

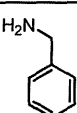
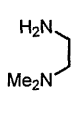
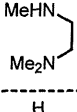
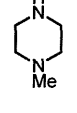
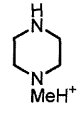
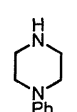
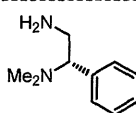
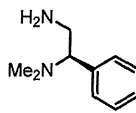
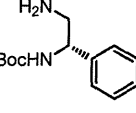
**Plan of the Design of Potent Agents.** In the *in silico* screening carried out in this study, 4 features, *i.e.*, hydrophobic region, hydrogen-bond donor, hydrogen-bond acceptor, and aromatic ring, were monitored for pharmacophore. Hit chemical compound 4 is compatible with stachyflin in the

three features of aromatic ring, hydrophobic region, and hydrogen-bond acceptor. Hit chemical compound 5 is compatible in all four features. All of the 8 selected compounds are compatible with stachyflin at least in two features, aromatic ring and hydrogen-bond acceptor. That is, these two features are commonly observed in pharmacophores of all selected compounds. This suggests that aromatic ring and hydrogen-bond acceptor are indispensable for inhibitors analogous to stachyflin. From the viewpoint of compatibility in the pharmacophore, compound 5 is the most advantageous for an HA inhibitor. In the binding modes of compounds 4 and 5 to the wild-type HA shown in Figure 3, compound 4 generated three hydrogen bonds with HA. In contrast, one hydrogen bond was observed between compound 5 and HA. The binding position of compound 5 is considerably close to that of stachyflin. These findings in binding mode suggest that the shape complementarity between compound 5 and the binding site in HA is high, while electrostatic complementarity is more significant in the binding of compound 4.

Methylester of compound 4 corresponds to carbonyl oxygen on ring E of stachyflin, and methoxy corresponds to the hydroxy group bound to ring D. It should be noted that rings DE of stachyflin compose a large flat region and that the vanillic acid core of compound 4 mimics the flat region and the distribution of polar atoms. Diazolane of compound 4 is compatible with ring A of stachyflin, and amine on the

**Table 3. Structures and Inhibitory Activities of the Synthesized Analogues to Compound 5, Which Bears a Thieno-pyrimidine Core<sup>a</sup>**



| Compound | Amine   | Yield (%) | EC <sub>50</sub> (μM) |
|----------|---|-----------|-----------------------|
| 31       |    | 45        | 3.6                   |
| 32       |    | 62        | >10                   |
| 33       |    | 43        | >10                   |
| -----    |   |           |                       |
| 34       |   | 54        | >10                   |
| 35       |  | 28        | 0.6                   |
| 36       |  | 82        | 4.6                   |
| -----    |   |           |                       |
| 37       |  | 48        | 2.0                   |
| 38       |  | 32        | >10                   |
| 39       |  | 7         | 4.8                   |

<sup>a</sup>Condition: (b) amine, NaOH, THF, reflux, 6 h.

diazolane corresponds to the hydroxy group bound to ring A. Compound 9 in Table 2, in which diazolane is replaced by methoxy, shows a considerably high inhibitory activity. Therefore, a polar group at the position of the diazolane is not necessarily required to maintain compound potency.

Sulfur and nitrogen atoms of thieno-pyrimidine moiety of compound 5 mimic the charge distribution of rings DE. It is notable that thieno-pyrimidine also composes a large flat

region. Another thiophene and dimethylamine are compatible with rings A and B of stachyflin, respectively. The high inhibitory activity of compound 35 in Table 3 suggests that thiophene is not necessarily required to maintain compound potency. This finding provides a sound explanation for the high inhibitory activity of compound 9. Accordingly, the region of ring A of stachyflin is not so important for inhibitory activity. Instead, the flat region at rings DE and the charge distribution on the flat region are essential for compound potency.

Compound 9 and 35 were docked to the wild-type HA and the three mutants in the same manner as stachyflin was. The predicted binding structures in Supplementary Figure S8 indicate that the binding site of compound 9 changed among the models. In contrast, compound 35 was bound to almost the same location among all models. The thieno-pyrimidine moiety is positioned near D109. This position is, however, different from that of stachyflin. The sizes of compounds 9 and 35 are small compared to stachyflin and compounds 4 and 5. Hence this smallness may be a reason for the incompatibility of the binding mode. To produce potent compounds appropriately fitted to the domain between inner helices of HA, compounds 9 and 35 should be converted with retention of the vanillic acid core and/or the thieno-pyrimidine moiety and with attachment of some chemical group containing a chiral center at the opposite side to cling to the helix round surface.

## METHODS

**Molecular Dynamics Simulation.** Information on the structural difference between the wild-type HA and the mutants is essential for clarifying the reason why some amino acid mutations in HA diminish the inhibitory activity of stachyflin. The initial structure of the wild-type HA of WSN strain was constructed by homology modeling using Modeler ver. 9.4.<sup>37</sup> The multiple-alignment technique was employed, where the X-ray crystal structures of A/Puerto Rico/8/1934 H1N1 with PDB codes 1RVZ and 1RU7<sup>38</sup> and A/Brevig Mission/1/1918 H1N1 with code 1RD8<sup>39</sup> were selected for references in modeling. Homology modeling was also performed to build the initial structures for variants; K51R and K121E mutations were introduced in the HA2 subunit in mutant 1, V176I in HA1 and K51R, K121E in HA2 in mutant 2, and V176I in HA1 and K51R in HA2 in mutant 3. A lipid bilayer of 100 Å × 100 Å was generated by using an in-house software GLYMM implemented in VMD ver. 1.8<sup>40</sup> for the purpose of embedding the C-terminal side of HA2 subunit into the lipid membrane mimicking the viral envelope. The composition of lipid molecules in the membrane was set to be as compatible as possible with the composition of lipid molecules in the influenza viral envelope, as shown in Supplementary Table 1. Judging from the prediction results with UniProtKB,<sup>41</sup> amino residues 186–206 were assumed to be the transmembrane region embedded in the viral envelope. It is natural to consider that an α helix structure is formed in the transmembrane region. However, there is no experimental ground for the formation of an α helix in this region. Accordingly, this region was set to have no secondary structure, that is, to be in a strand form in the initial structure of the present simulations. In our preliminary calculation without embedding the C-terminal side of HA2 subunit into the lipid membrane, each helix in HA2 gradually changed its conformation to separate itself from other helices. HA trimer was converted from a closed shape to an open one with the progress of simulation. The motion of the C-terminal region of HA2 was large in the preliminary calculation, which seemed to be a cause of structural instability and became a trigger for the drastic conformational change. That is, the helices of the HA trimer cannot maintain the closed form unless the C-terminal side of HA2 is embedded in the lipid membrane. Hence, calculation models in this work included the membrane mimicking the viral envelope and the transmembrane region of HA. TIP3P water molecules and ions to neutralize the calculation cell were generated to solvate the complex of HA and lipid membrane, making a



periodic boundary box of  $100 \text{ \AA} \times 100 \text{ \AA} \times 250 \text{ \AA}$  in which the top and bottom parts of HA were set apart from the boundary by more than  $10 \text{ \AA}$  (Figure 1c). Consequently, the total number of atoms was about 259,300 in each model.

MD simulations were carried out for every model using NAMD ver. 2.6.<sup>42</sup> Initially, energy minimization was executed for 1,000,000 steps with the conjugate gradient method. Next, the temperature of the model system was elevated up to 310 K. Then 30 ns equilibrating simulation was performed in the NTP ensemble condition to obtain the equilibrated structures of the wild-type HA and the three kinds of mutants. Nonbonded interaction terms were computed with a cutoff distance of  $12 \text{ \AA}$ , where a switching distance of  $10 \text{ \AA}$  was applied to make the nonbonded interaction zero at the cutoff distance smoothly. A periodic boundary condition was applied to all directions of the calculation cell, and the particle mesh Ewald method was employed to compute the long-distance nonbonded interaction. CHARMM27 force field<sup>43</sup> was adopted for all atoms.

**Docking Simulation.** The binding modes of stachyflin to the wild-type HA and its mutants were predicted by docking simulation using GOLD ver. 4.<sup>44,45</sup> The equilibrated structure obtained from the MD simulation was utilized as a plausible protein structure of HA in the wild-type and three mutants. Binding score was also calculated to evaluate the difference in binding affinity due to the mutations. A preliminary docking calculation was executed to search for the docking area within  $30 \text{ \AA}$  from Phe110 of the HA2 subunit. Since an adequate docking space was found inside the area and stachyflin was positioned near Asp109 in the binding mode ranking first, recalculation of stachyflin docking was performed with the search area set within  $10 \text{ \AA}$  from Asp109 of HA2 subunit. Fifty binding poses were generated and the binding affinities of those binding poses were estimated by GOLD score function. On the basis of the ranking in the estimated GOLD score, the most probable binding pose was selected. The binding affinity for the selected binding pose was re-estimated using ASP score function. This two-step approach, *i.e.*, determination of the binding pose with GOLD score and subsequent estimation of binding affinity with ASP score, was reported to successfully provide reliable prediction in docking of low-molecular-weight ligands to an enzyme or receptor.<sup>46,47</sup>

**In Silico Screening.** A search for compounds bearing chemical features similar to those of stachyflin was made by an *in silico* pharmacophore screening. A chemical database was provided by Namiki Co. Ltd., in which about 3 million synthesized compounds are listed and all of the compounds are available by purchase. First, conformations of every compound were generated by using OMEGA module of OpenEye software.<sup>48</sup> Totally, more than 200 million chemical conformations were generated. Second, the pharmacophore of stachyflin was extracted for setting queries, in which hydrogen-bond donor and acceptor, aromatic ring, and hydrophobic region appeared to be key features. Third, chemical screening was carried out from the viewpoint of structural similarity to stachyflin using ROCS module of OpenEye.<sup>49</sup> A total of 5094 compounds were extracted from the Namiki database under the condition of the Tanimoto coefficient being more than 0.75. Fourth, more condensed selection of chemicals from the 5094 compounds was performed using EON module<sup>49</sup> from the viewpoint of similarity in charge distribution. The compounds without structural flexibility were excluded. Consequently, 8 chemical compounds were selected as candidates for purchase.

**Synthesis of Analogue Compounds.** Two series of derivatives were synthesized in this work. One is an analogue containing a vanillic acid skeleton, and the other is one bearing thieno-pyrimidine. Compound 9, 3-methoxy-4-[(methyl-sulfonyl)oxy]-benzoic acid methoxy-ester, is a typical derivative of the former series. A mixture of vanillic acid methyl (1.0 g, 5.49 mmol),  $\text{KCO}_3$  (1.13 g, 8.24 mmol), and acetonitrile (30 mL) was cooled in an ice bath under Ar atmosphere. Methane-sulfonyl chloride (0.51 mL, 6.59 mmol) was slowly added to the mixture, and then the solution was mechanically stirred for 3 h at RT. The reaction mixture was filtered with Celite, and the solvent was removed *in vacuo*. The resulting product was extracted with a solution of EtOAc (30 mL) and 1 M aqueous HCl (30 mL). The aqueous layer was treated with EtOAc (20 mL) two times, and

the combined organic layer was washed with brine, dried over  $\text{MgSO}_4$ , and concentrated *in vacuo*. The product was purified by thin-layer chromatography with hexane/EtOAc in a ratio of 3:1. The solid obtained was resuspended with a solution of hexane and EtOAc, and recrystallization produced the final compound as a white solid (1.01 g, yield 71%).

A typical derivative of the latter series is compound 3S, 4-(4-methyl-1-piperazinyl)-thieno[2,3-*d*]pyrimidine hydrochloride salt. 4-Chloro-thieno[2,3-*d*]pyrimidine (200 mg, 1.17 mmol) was solvated with THF (15 mL). After addition of 1-methyl-piperazine (0.26 mL, 2.34 mmol) and NaOH (0.94 g, 2.34 mmol), the mixture was heated under reflux for 6 h. The solvent was removed *in vacuo*, and the reaction mixture was treated with a solution of EtOAc (20 mL) and distilled  $\text{H}_2\text{O}$  (15 mL). The product was extracted with EtOAc two times, and the organic layer was washed with brine and dried over  $\text{Na}_2\text{SO}_4$ . The solvent was evaporated *in vacuo*, and the resulting product was purified by two-dimensional thin-layer chromatography with hexane/EtOAc in ratios of 3:1 and 1:1. A brown solid of (phenyl piperazinyl)-thienopyrimidine was obtained in a yield of 54% (148 mg). The solid obtained was resuspended in a solution of toluene (20 mL) and 1 M aqueous HCl (0.6 mL) and heated under reflux for 1 h. The reaction solution was cooled to RT, and filtration gave the final compound as a brownish solid (127 mg, yield 45%).

**Antiviral Assay.** Compound potency was tested by an influenza virus cell culture assay with measurement of the quantity of viral RNA using real-time polymerase chain reaction (RT-PCR). Test compounds were mixed with minimum essential medium (MEM) containing bovine serum albumin (BSA). To prepare a virus-containing compound-mixed medium, 100 units of 50% tissue culture infective dose (TCID<sub>50</sub>) of influenza virus A/Puerto Rico/8/34 strain (PR8) was suspended in 100  $\mu\text{L}$  of the MEM-BSA containing test compounds and 10  $\mu\text{g}/\text{mL}$  of acetylated trypsin. Madin-Darby canine kidney (MDCK) cells were loaded in a 96-well plate. The cells were washed with phosphate-buffered saline (PBS), followed by 0.5–1 h incubation with compound-mixed medium. The virus-containing compound-mixed medium was also incubated for 0.5–1 h. After incubation, MDCK cells in the compound-mixed medium without viruses were transferred to the compound-mixed medium with viruses. Then the cells were incubated for 1 h at 37 °C in 100  $\mu\text{L}$  of the virus-containing compound-mixed medium (100 TCID<sub>50</sub> influenza virus, 10  $\mu\text{g}/\text{mL}$  acetylated trypsin, and test compound at several concentrations). MDCK cells were washed with compound-mixed medium without viruses and incubated in the compound-mixed, acetylated trypsin-containing medium without influenza virus for 24 h. Culture supernatants of MDCK cells were collected after the incubation, and RNA was extracted from the supernatants. The amount of viral RNA was measured by the RT-PCR method. The measurement was compared to that of the control that was performed in a similar manner without any test compound. The compound concentration to suppress viral proliferation to 50% (EC<sub>50</sub>) was estimated from the comparison.

**RNA Extraction and RT-PCR.** To monitor the efficiency of RNA purification, uninfected VeroE6 cells were mixed in the ISOGEN reagent as a source of 18S rRNA for normalization. Supernatants from MDCK cell culture medium were mixed with ISOGEN reagent and RNA was purified according to the manufacturer's protocol. For quantification of PR8 HA RNA, real-time RT-PCR was performed using the primers and the probe with the sequences of PR8-HA-F: 5'-GGCAAATGGAAATCTAATAGCACC-3', PR8-HA-R: 5'-TGATGCTTTTGAGGTGATGA-3', and PR8-HA-probe: 5'-FAM-TCCGACTGAGTAGAGGCTTTGGGTCC-TAMRA-3'. For monitoring efficiency of RNA purification, 18S rRNA was quantified using the primers and the probe with the sequences of 18S-F: 5'-GTAACCCGTTGAACCCCAT-3', 18S-R: 5'-CCATCCAATCGGTAGTAGCG-3', and 18S-probe: 5'-FAM-TGCGTTGAT-TAAGTCCCTGCCCTTTGTA-TAMRA-3'. The intensity of fluorescence emitted from the probe was detected by the ABI-7700 sequence detector system (Applied Biosystems).

## ■ ASSOCIATED CONTENT

## ● Supporting Information

Composition of lipid membrane models, predicted binding affinities, RMSDs during MD simulation, predicted binding structures of stachyflin, superimposition of HA structures, chemical properties of synthesized compounds, and their NMR spectra. This material is available free of charge via the Internet at <http://pubs.acs.org>.

## ■ AUTHOR INFORMATION

## Corresponding Author

\*E-mail: (N.Y.) [n-yama-5@nih.go.jp](mailto:n-yama-5@nih.go.jp); (T.H.) [hoshino@chiba-u.jp](mailto:hoshino@chiba-u.jp).

## Author Contributions

#These authors contributed equally to this work.

## ■ ACKNOWLEDGMENTS

We thank L.Q. Mai (National Institute of Hygiene and Epidemiology, Hanoi) for providing the A/Vietnam/1194/04 virus strain. This work was partly supported by a Health and Labor Science Research Grant for Research from the Ministry of Health and Labor of Japan. This work was also supported by a Grant-in-Aid for Scientific Research (C) from Japan Society for the Promotion of Science (JSPS). This study was also supported in part by a grant-in-aid (S0991013) from the Ministry of Education, Culture, Sport, Science, and Technology, Japan (MEXT) for the Foundation of Strategic Research Projects in Private Universities. Theoretical calculations were performed at the Research Center for Computational Science, Okazaki, Japan and at the Information Technology Center of the University of Tokyo and also by the high-performance computer system at Institute for Media Information Technology in Chiba University.

## ■ REFERENCES

- (1) Gambotto, A.; Barratt-Boyes, S. M.; de Jong, M. D.; Neumann, G.; and Kawaoka, Y. (2008) Human infection with highly pathogenic H5N1 influenza virus. *Lancet* 371, 1464–1475.
- (2) Beigel, J. H., Farrar, J., Han, A. M., Hayden, F. G., Hyer, R., de Jong, M. D., Lochindarat, S., Nguyen, T. K. T., Nguyen, T. H., Tran, T. H., Nicoll, A., Touch, S., Yuen, K. Y., and Writing Committee of the World Health Organization Consultation on Human Influenza A/H5. (2005) Avian influenza A (H5N1) infection in humans. *N. Engl. J. Med.* 353, 1374–1385.
- (3) Schnell, J. R., and Chou, J. J. (2008) Structure and mechanism of the M2 proton channel of influenza A virus. *Nature* 451, 591–595.
- (4) Stouffer, A. L., Acharya, R., Salom, D., Levine, A. S., Di Costanzo, L., Soto, C. S., Tereshko, V., Nanda, V., Stayrook, S., and DeGrado, W. F. (2008) Structural basis for the function and inhibition of an influenza virus proton channel. *Nature* 451, 596–599.
- (5) McNicholl, I. R., and McNicholl, J. J. (2001) Neuraminidase inhibitors: zanamivir and oseltamivir. *Ann. Pharmacother.* 35, 57–70.
- (6) Moscona, A. (2005) Neuraminidase inhibitors for influenza. *N. Engl. J. Med.* 353, 1363–1373.
- (7) Bright, R. A., Medina, M.-j., Xu, X., Perez-Orozco, G., Wallis, T. R., Davis, X. M., Povinelli, L., Cox, N. J., and Klimov, A. I. (2005) Incidence of adamantane resistance among influenza A (H3N2) viruses isolated worldwide from 1994 to 2005: a cause for concern. *Lancet* 366, 1175–1181.
- (8) Deyde, V. M., Xu, X., Bright, R. A., Shaw, M., Smith, C. B., Zhang, Y., Shu, Y., Gubareva, L. V., Cox, N. J., and Klimov, A. I. (2007) Surveillance of resistance to adamantanes among influenza A(H3N2) and A(H1N1) viruses isolated worldwide. *J. Infect. Dis.* 196, 249–257.
- (9) Kitahori, Y., Imanishi, Y., and Inoue, Y. (2008) High incidence of amantadine-resistant influenza H1N1 viruses isolated during the 2007–2008 season in Nara Prefecture, Japan. *Jpn. J. Infect. Dis.* 61, 253–254.
- (10) Kamigauchi, T.; Fujiwara, T.; Tani, H.; Kawamura, Y.; Horibe, I. Shionogi & Co, Ltd. Sesquiterpene derivatives having antiviral activity, Patent WO/1997/011947, 1997.
- (11) Taishi, T., Takechi, S., and Mori, S. (1998) First total synthesis of ( $\pm$ )-stachyflin. *Tetrahedron Lett.* 39, 4347–4350.
- (12) Yoshimoto, J., Kakui, M., Iwasaki, H., Fujiwara, T., Sugimoto, H., and Hattori, N. (1999) Identification of a novel HA conformational change inhibitor of human influenza virus. *Arch. Virol.* 144, 865–878.
- (13) Yoshimoto, J., Kakui, M., Iwasaki, H., Sugimoto, H., Fujiwara, T., and Hattori, N. (2000) Identification of amino acids of influenza virus HA responsible for resistance to a fusion inhibitor, Stachyflin. *Microbiol. Immunol.* 44, 677–685.
- (14) Rosenbaum, D. M., Cherezov, V., Hanson, M. A., Rasmussen, S. G. F., Thian, F. S., Kobilka, T. S., Choi, H. J., Yao, H. J., Weis, W. I., Stevens, R. C., and Kobilka, B. K. (2007) GPCR engineering yields high-resolution structural insights into  $\beta$ 2-adrenergic receptor function. *Science* 318, 1266–1273.
- (15) Wegener, A. A., Klare, J. P., Engelhard, M., and Steinhoff, H. J. (2001) Structural insights into the early steps of receptor-transducer signal transfer in archaeal phototaxis. *EMBO J.* 20, 5312–5319.
- (16) Sato, Y., Hata, M., Neya, S., and Hoshino, T. (2005) Computational analysis of the transient movement of helices in sensory rhodopsin II. *Protein Sci.* 14, 183–192.
- (17) Cross, K. J., Burleigh, L. M., and Steinhauer, D. A. (2001) Mechanisms of cell entry by influenza virus. *Exp. Rev. Mol. Med.* 3, 1–15.
- (18) Bodian, D. L., Yamasaki, R. B., Buswell, R. L., Stearns, J. F., White, J. M., and Kuntz, I. D. (1993) Inhibition of the fusion-inducing conformational change of influenza hemagglutinin by benzoquinones and hydroquinones. *Biochemistry* 32, 2967–2978.
- (19) Luo, G., Colonna, R., and Krystal, M. (1996) Characterization of hemagglutinin-specific inhibitor of influenza A virus. *Virology* 226, 66–76.
- (20) Plotch, S. J., O'Hara, B., Morin, J., Palant, O., LaRocque, J., Bloom, J. D., Lang, S. A. Jr., DiGrandi, M. J., Bradley, M., Nilakantan, R., and Gluzman, Y. (1999) Inhibition of influenza A virus replication by compounds interfering with the fusogenic function of the viral hemagglutinin. *J. Virol.* 73, 140–151.
- (21) Staschke, K. A., Hatch, S. D., Tang, J. C., Hornback, W. J., Munroe, J. E., Colacino, J. M., and Muesing, M. A. (1998) Inhibition of influenza virus hemagglutinin-mediated membrane fusion by a compound related to podocarpic acid. *Virology* 248, 264–274.
- (22) Hoffman, L. R., Kuntz, I. D., and White, J. M. (1997) Structure-based identification of an inducer of the low-pH conformational change in the influenza virus hemagglutinin: Irreversible inhibition of infectivity. *J. Virol.* 71, 8808–8820.
- (23) Matsubara, T., Onishi, A., Saito, T., Shimada, A., Inoue, H., Taki, T., Nagata, K., Okahata, Y., and Sato, T. (2010) Sialic acid-mimic peptides as hemagglutinin inhibitors for anti-influenza therapy. *J. Med. Chem.* 53, 4441–4449.
- (24) Feng, F., Miura, N., Isoda, N., Sakoda, Y., Okamatsu, M., Kida, H., and Nishimura, S. (2010) Novel trivalent anti-influenza reagent. *Bioorg. Med. Chem. Lett.* 20, 3772–3776.
- (25) Tang, G., Lin, X., Qiu, Z., Li, W., Zhu, L., Wang, L., Li, S., Li, H., Lin, W., Yang, M., Guo, T., Chen, L., Lee, D., Wu, J. Z., and Yang, W. (2011) Design and synthesis of benzenesulfonamide derivatives as potent anti-influenza hemagglutinin inhibitors. *ACS Med. Chem. Lett.* 2, 603–607.
- (26) Sawada, T., Fedorov, D. G., and Kitaura, K. (2010) Role of the key mutation in the selective binding of avian and human influenza hemagglutinin to sialosides revealed by quantum-mechanical calculations. *J. Am. Chem. Soc.* 132, 16862–16872.
- (27) Takematsu, K., Fukuzawa, K., Omagari, K., Nakajima, S., Nakajima, K., Mochizuki, Y., Nakano, T., Watanabe, H., and Tanaka, S. (2009) Possibility of mutation prediction of influenza hemagglutinin



by combination of hemadsorption experiment and quantum chemical calculation for antibody binding. *J. Phys. Chem. B* 113, 4991–4994.

(28) Newhouse, E. I., Xu, D., Markwick, P. R., Amaro, R. E., Pao, H. C., Wu, K. J., Alam, M., McCammon, J. A., and Li, W. W. (2009) Mechanism of glycan receptor recognition and specificity switch for avian, swine, and human adapted influenza virus hemagglutinins: a molecular dynamics perspective. *J. Am. Chem. Soc.* 131, 17430–17442.

(29) Kasson, P. M., Ensign, D. L., and Pande, V. S. (2009) Combining molecular dynamics with bayesian analysis to predict and evaluate ligand-binding mutations in influenza hemagglutinin. *J. Am. Chem. Soc.* 131, 11338–11340.

(30) Das, P., Li, J., Royyuru, A. K., and Zhou, R. (2009) Free energy simulations reveal a double mutant avian H5N1 virus hemagglutinin with altered receptor binding specificity. *J. Comput. Chem.* 30, 1654–1663.

(31) Xu, D., Newhouse, E. I., Amaro, R. E., Pao, H. C., Cheng, L. S., Markwick, P. R., McCammon, J. A., Li, W. W., and Arzberger, P. W. (2009) Distinct glycan topology for avian and human sialopentaccharide receptor analogues upon binding different hemagglutinins: a molecular dynamics perspective. *J. Mol. Biol.* 387, 465–491.

(32) Fleishman, S. J., Whitehead, T. A., Ekiert, D. C., Dreyfus, C., Corn, J. E., Strauch, E. M., Wilson, I. A., and Baker, D. (2011) Computational design of proteins targeting the conserved stem region of influenza hemagglutinin. *Science* 332, 816–821.

(33) Watanabe, K., Sakurai, J., Abe, H., and Katoh, T. (2010) Total synthesis of (+)-stachyflin: a potential anti-influenza A virus agent. *Chem. Commun.* 46, 4055–4057.

(34) Nakatani, M., Nakamura, M., Suzuki, A., Inoue, M., and Katoh, T. (2002) A new strategy toward the total synthesis of stachyflin, a potent anti-influenza A virus agent: concise route to the tetracyclic core structure. *Org. Lett.* 4, 4483–4486.

(35) Carey, J. S., Laffan, D., Thomson, C., and Williams, M. T. (2006) Analysis of the reactions use for the preparation of drug candidate molecules. *Org. Biomol. Chem.* 4, 2337–2347.

(36) Mizukami, T., Imai, J., Hamaguchi, I., Kawamura, M., Momose, H., Naito, S., Maeyama, J., Masumi, A., Kuramitsu, M., Takizawa, K., Nomura, N., Watanabe, S., and Yamaguchi, K. (2008) Application of DNA microarray technology to influenza A/Vietnam/1194/2004 (H5N1) vaccine safety evaluation. *Vaccine* 26, 2270–2283.

(37) Sali, A., and Blundell, T. L. (1993) Comparative protein modelling by satisfaction of spatial restraints. *J. Mol. Biol.* 234, 779–815.

(38) Gamblin, S. J., Haire, L. F., Russell, R. J., Stevens, D. J., Xiao, B., Ha, Y., Vasisht, N., Steinhauer, D. A., Daniels, R. S., Elliot, A., Wiley, D. C., and Skehel, J. J. (2004) The structure and receptor binding properties of the 1918 influenza hemagglutinin. *Science* 303, 1838–1842.

(39) Stevens, J., Corper, A. L., Basler, C. F., Taubenberger, J. K., Palese, P., and Wilson, I. A. (2004) Structure of the uncleaved human H1 hemagglutinin from the extinct 1918 influenza virus. *Science* 303, 1866–1870.

(40) Humphrey, W., Dalke, A., and Schulten, K. (1996) VMD: visual molecular dynamics. *J. Mol. Graph.* 14, 33–38.

(41) The UniProt Consortium. (2011) Ongoing and future developments at the Universal Protein Resource. *Nucleic Acids Res.* 39, D214–D219.

(42) Phillips, J. C., Braun, R., Wang, W., Gumbart, J., Tajkhorshid, E., Villa, E., Chipot, C., Skeel, R. D., Kalé, L., and Schulten, K. (2005) Scalable molecular dynamics with NAMD. *J. Comput. Chem.* 26, 1781–1802.

(43) Feller, S. E., Gawrisch, K., and MacKerell, A. D. (2002) Polyunsaturated fatty acids in lipid bilayers: intrinsic and environmental contributions to their unique physical properties. *J. Am. Chem. Soc.* 124, 318–326.

(44) Jones, G., Willett, P., Glen, R. C., Leach, A. R., and Taylor, R. (1997) Development and validation of a genetic algorithm for flexible docking. *J. Mol. Biol.* 267, 727–748.

(45) Jones, G., Willett, P., and Glen, R. C. (1995) Molecular recognition of receptor sites using a genetic algorithm with a description of desolvation. *J. Mol. Biol.* 245, 43–53.

(46) Verdonk, M. L., Cole, J. C., Hartshorn, M. J., Murray, C. W., and Taylor, R. D. (2003) Improved protein-ligand docking using GOLD. *Proteins: Struct., Funct., Genet.* 52, 609–623.

(47) Mooij, W. T. M., and Verdonk, M. L. (2005) General and targeted statistical potentials for protein-ligand interactions. *Proteins: Struct., Funct., Genet.* 61, 272–281.

(48) Bostrom, J., Greenwood, J. R., and Gottfries, J. (2003) Assessing the performance of OMEGA with respect to retrieving bioactive conformations. *J. Mol. Graphics Modell.* 21, 449–462.

(49) OpenEye Scientific Software, Inc., Santa Fe, NM, USA, www.eyesopen.com.

# Entry of Human T-Cell Leukemia Virus Type 1 Is Augmented by Heparin Sulfate Proteoglycans Bearing Short Heparin-Like Structures

Atsushi Tanaka,<sup>a</sup> Atsushi Jinno-Oue,<sup>a</sup> Nobuaki Shimizu,<sup>a</sup> Ariful Hoque,<sup>a</sup> Takahisa Mori,<sup>a</sup> Salequl Islam,<sup>a</sup> Youko Nakatani,<sup>a</sup> Masahiko Shinagawa,<sup>b</sup> and Hiroo Hoshino<sup>a</sup>

Department of Virology and Preventive Medicine, Gunma University Graduate School of Medicine, Maebashi, Gunma, Japan,<sup>a</sup> and Institute for Genetic Medicine, Hokkaido University, Hokkaido, Japan<sup>b</sup>

Three molecules have been identified as the main cellular factors required for binding and entry of human T-cell leukemia virus type 1 (HTLV-1): glucose transporter 1 (GLUT1), heparan sulfate (HS), and neuropilin 1 (NRP-1). However, the precise mechanism of HTLV-1 cell tropism has yet to be elucidated. Here, we examined the susceptibilities of various human cell lines to HTLV-1 by using vesicular stomatitis virus pseudotypes bearing HTLV-1 envelope proteins. We found that the cellular susceptibility to HTLV-1 infection did not correlate with the expression of GLUT1, HS, or NRP-1 alone. To investigate whether other cellular factors were responsible for HTLV-1 susceptibility, we conducted expression cloning. We identified two HS proteoglycan core proteins, syndecan 1 and syndecan 2, as molecules responsible for susceptibility to HTLV-1. We found that treatment of syndecan 1-transduced cells (expressing increased HS) with heparinase, a heparin-degradative enzyme, reduced HTLV-1 susceptibility without affecting the expression levels of HS chains. To further elucidate these results, we characterized the expression of HS chains in terms of the mass, number, and length of HS in several syndecan 1-transduced cell clones as well as human cell lines. We found a significant correlation between HTLV-1 susceptibility and the number of HS chains with short chain lengths. Our findings suggest that a combination of the number and the length of HS chains containing heparin-like regions is a critical factor which affects the cell tropism of HTLV-1.

Human T-cell leukemia virus type 1 (HTLV-1) is the causative agent of adult T-cell leukemia (16, 49) and HTLV-1-associated myelopathy, also known as tropical spastic paraparesis (10, 24, 45). Previous investigations revealed that HTLV-1 infects not only human T lymphocytes and central nervous system cells but also cells of other tissues (6, 17, 21, 34, 51, 69). To date, glucose transporter 1 (GLUT1), neuropilin-1 (NRP-1), and heparan sulfate proteoglycans (HSPGs) have been implicated as being involved in HTLV-1 infection (reviewed in reference 12). The expression of GLUT1, which is responsible for viral binding and fusion mediated by the gp46 surface envelope (Env) protein (3, 26, 39), is ubiquitous, and it is also known that various cells express HSPGs. Although these findings might be able to explain the broad host cell range of HTLV-1, they are not sufficient to explain the variance of HTLV-1 cell tropism.

It was previously reported that HTLV-1 spreads from cell to cell via virological synapses (22, 38); however, recent studies by Pais-Correia and colleagues showed that the HTLV-1 virions retaining extracellular structures are important for HTLV-1 cell transmission (46). That study implied that the viral particle mediates HTLV-1 transmission and suggested the importance of the interaction between viral particles and the target cell surface. In this study, we investigated the susceptibilities of various human cell lines to cell-free HTLV-1 infection using highly infectious vesicular stomatitis virus (VSV) pseudotypes harboring the Env protein of HTLV-1. These pseudotype viruses express green fluorescent protein (GFP) in infected cells. We observed a >1,000-fold difference in the susceptibilities of these pseudotypes among the human cell lines. Interestingly, the levels of GLUT1 expression on the cell surface and the amount of cell surface heparan sulfate (HS) chains did not reflect susceptibility to HTLV-1 in human cell lines. In addition, the expression of NRP-1 mRNA also did not reflect susceptibility to HTLV-1. From these data, we suspected

the existence of an unknown factor that affects the interaction between these three molecules and the viral particles and causes the differences in cell tropism of the HTLV-1 particle. Therefore, we used an expression cloning method to investigate potential candidates and found that two HS proteoglycan (HSPG) core proteins, syndecan 1 and 2 (SDC1 and SDC2), play a significant role in cellular susceptibility to HTLV-1.

## MATERIALS AND METHODS

**Cell lines.** The human T-cell line Molt-4 clone 8 (29), the HTLV-1-positive but HTLV-1 Env-negative T-cell line C8166 (53), the HTLV-1-producing T-cell lines C91/PL (50) and MT-2 (41), and K562 cells transduced with the CD4 gene and ecotropic murine leukemia virus receptor gene (K562/CD4/ecoR; referred to here as K4R cells) (58) were all maintained in RPMI 1640 medium supplemented with 10% fetal bovine serum (FBS). The human astrocytoma cell line U251MG (2), the human glioma cell line NP-2 (58), the feline kidney fibroblast cell line S+L-CCC clone 8C (8), 8C cell lines persistently infected with the strains 2M (cosmopolitan strain) (18) and MEL5 (Melanesian strain) (11) of HTLV-1 (8C/HTLV-1<sub>2M</sub> and 8C/HTLV-1<sub>MEL5</sub>) (19, 20), and a fetal lamb kidney cell line that was persistently infected with bovine leukemia virus (BLV), FLK (67), were all maintained in Eagle's minimum essential medium (MEM) supplemented with 10% FBS. The human osteosarcoma-derived cell line HOS (40), the human colon cancer cell line HT-29 (55), the human renal epithelial cell line expressing adenovirus E1a and SV40 large T antigen, 293T (14, 47), and the retrovirus-packaging cell lines Plat-E (42) and

Received 25 July 2011 Accepted 3 January 2012

Published ahead of print 11 January 2012

Address correspondence to Atsushi Tanaka, atsushit@med.gunma-u.ac.jp.

Copyright © 2012, American Society for Microbiology. All Rights Reserved.

doi:10.1128/JVI.05783-11

Phoenix-A (31) (kindly provided by T. Kitamura [Institute of Medical Science, The University of Tokyo, Tokyo, Japan] and G. Nolan [Stanford University, Stanford, CA], respectively) were maintained in Dulbecco's modified MEM supplemented with 10% FBS.

**Preparation of VSVΔG\*-G and VSVΔG\* pseudotypes.** In this study, we used VSVΔG\* pseudotypes bearing the VSV-G protein and BLV Env [VSVΔG\*(HTLV-1<sub>MEL5</sub>), VSVΔG\*(HTLV-1<sub>2M</sub>), and VSVΔG\*(BLV)] as the controls for VSVΔG\* pseudotypes bearing HTLV-1 Env. Both of these viruses infect various mammalian cell lines similarly to HTLV-1, although their cellular receptors have yet to be identified. BLV and HTLV are ~50% similar at the nucleotide level and share many common features; however, BLV is known to use a different cellular receptor (59).

Recombinant VSV, VSVΔG\*-G, was kindly provided by M. A. Whitt (University of Tennessee, Memphis, TN) (62). VSVΔG\*-G was inoculated into 293T cells that had been transfected with an expression plasmid of VSV G protein, pCAGGS/VSVG. Culture supernatants containing newly propagated VSVΔG\*-G were harvested after incubation for 24 to 30 h at 37°C. 8C/HTLV-1<sub>MEL5</sub>, 8C/HTLV-1<sub>2M</sub>, or FLK cells were plated on 100-mm plates and inoculated 1 day later with VSVΔG\*-G at a multiplicity of infection of 5 to 10 (when titrated on 8C cells) for 1 to 2 h at 37°C. The cells were washed with medium, and then medium supplemented with 2% FBS and 50 mM HEPES (pH 7.1) was added. Culture supernatants containing propagated VSVΔG\* pseudotypes bearing HTLV-1 Env [VSVΔG\*(HTLV-1)] or BLV Env [VSVΔG\*(BLV)] were harvested after 18 to 24 h of incubation at 33°C in a CO<sub>2</sub> incubator. Culture supernatant containing the VSVΔG\*-G or VSVΔG\* pseudotype was clarified by low-speed centrifugation, and aliquots of the supernatant were stored at -80°C until use.

Prior to inoculation, VSVΔG\*(HTLV-1) and VSVΔG\*(BLV) samples were incubated with ~2 to 10% anti-VSV serum, which was obtained from a goat that had been repeatedly immunized with VSV, for 20 min at 30°C to completely neutralize the remaining VSVΔG\*-G. After 20 to 30 h of inoculation, the number of GFP-expressing cells was counted under a fluorescence microscope. Because of the absence of secondary infection by descendant VSVΔG\* pseudotypes, the number of GFP-positive cells was the same as the number of infectious units (IUs) of VSVΔG\* pseudotypes. The viral susceptibility of each cell was evaluated by the IUs obtained by inoculation with 1 ml VSVΔG\* pseudotype. Serum (0.2%) from an HTLV-1-infected healthy carrier or a rat anti-gp46 monoclonal antibody (MAb), LAT-27 (a generous gift from Y. Tanaka, Ryuky University, Nichihara, Okinawa, Japan) (15, 63), was used to neutralize VSVΔG\*(HTLV-1). Anti-BLV serum (~0.5 to 1%) from leukemic cattle was used to neutralize VSVΔG\*(BLV). Neutralizations of VSVΔG\*(HTLV-1) and VSVΔG\*(BLV) by antisera and MAbs were carried out simultaneously with an anti-VSV serum treatment step; i.e., pseudotype viruses were treated with anti-VSV serum in the presence or absence of anti-HTLV-1 (or BLV) serum for 20 min at 30°C. Formation of each pseudotype was confirmed by an almost complete neutralization using specific antisera or MAbs against each virus.

**Molecular cloning and sequencing of cDNA responsible for increased HTLV-1 susceptibility.** Poly(A)<sup>+</sup> RNA was extracted from the highly HTLV-1-susceptible U251MG cells using a FastTrack kit (Invitrogen, Carlsbad, CA). The RNA was then used to synthesize a cDNA library using the SuperScript Choice system for cDNA synthesis (Invitrogen). This cDNA library was cloned into the retroviral vector pMXpuro (44) according to the protocol of Kitamura and colleagues (32). The resultant expression cDNA library, pMXpuro/U251MG-cDNA, was then transfected into Plat-E cells (2 × 10<sup>6</sup> cells in a 60-mm culture plate) using the Fugene6 transfection reagent (Roche, Indianapolis, IN). Thirty-four hours after transfection, the culture supernatant containing the retroviral library was harvested and then inoculated into 1 × 10<sup>6</sup> K4R cells in the presence of Polybrene (10 μg/ml).

Genomic DNA extracted from isolated cell clones that showed an increased susceptibility to VSVΔG\*(HTLV-1<sub>MEL5</sub>) compared with parental K4R cells was subjected to PCR to recover the introduced cDNAs. The following PCR primers were used, which were derived from the pMXpuro

vector sequences flanking the inserted cDNAs: 5'-GGACCATCCTCTAG ACTGCCGGATCCCAGTGTG-3' and 5'-ATACTTCTGCCTGCTGGG GAGCCTGGGGAC-3'. PCR was performed using LA *Taq* polymerase (Takara Shuzo Co., Ltd., Ohtsu, Shiga, Japan) under the following conditions: 1 cycle at 94°C for 2 min, then 35 cycles at 98°C for 20 s and 68°C for 5 min, and one final cycle at 68°C for 5 min. PCR-amplified fragments were purified using a GeneClean II kit (Bio 101, Inc., La Jolla, CA) and then cloned into the pCR2.1 TA vector (Invitrogen). The resultant plasmids were sequenced using a dye primer and a DNA sequencer SQ5050 (Hitachi, Tokyo, Japan). The cloned sequences were analyzed for identity and similarity to other known sequences using the on-line BLAST program (28).

**Reverse transcriptase PCR and real-time PCR.** SDC1, SDC2, SDC3, SDC4, glypican 1 (GPC1), and NRP-1 mRNAs were detected by reverse transcription-PCR (RT-PCR). Total RNA was extracted from 293T, C8166, HOS, K4R, Molt-4, and U251MG cells using an RNA extraction kit (Isogen; Nippongene Co., Ltd., Tokyo, Japan) according to the manufacturer's protocol. For each sample, 4 μg of total RNA was subjected to an RT reaction using the SuperScript III first-strand synthesis system for RT-PCR (Invitrogen) according to the manufacturer's protocol. First-strand cDNA was then diluted to 50 μl using Tris-EDTA buffer (pH 8.0), and 1 μl was used as the template for PCR.

The relative NRP-1 mRNA levels were quantified in duplicate by quantitative PCR (qPCR) in the Mx3000P real-time PCR system (Agilent Technologies, CA) with brilliant SYBR green QPCR Master Mix (Agilent Technologies-Stratagene, CA), according to the manufacturer's instructions. qPCR mixtures were preincubated at 95°C for 10 min, followed by 40 cycles of PCR at 95°C for 30 s, 50°C for 30 s, and 72°C for 30 s, using the specific primer pair NRP-1/sense (5'-CCC GCACCTCATTCCATCATC-3'; positions 1946 to 1966) and NRP-1/antisense (5'-CATTTCATCCACC AAGTTCGCCG-3'; positions 2311 to 2331) (GenBank accession no. NM\_003873.5). The NRP-1 mRNA level in each cell line was normalized to human glyceraldehyde-3-phosphate dehydrogenase (GAPDH) mRNA using a predesigned Perfect real-time primer set for GAPDH (primer set identification HA031578; Takara Shuzo) and reported as the change (fold) compared with that from K4R cell data using the comparative quantitation analysis MxPro QPCR software available with Mx3000P.

PCR was performed with each specific primer pair to amplify the corresponding sequence. The codes and sequences of the PCR primers for the SDC1, SDC2, SDC3, SDC4, GPC1, and GLUT1 genes areas follows: SDC1/sense, 5'-GGTCCGGGCAGCATGAGGCGCGCGGCGCTC-3' (positions 288 to 317), and SDC1/antisense, 5'-CGCATGGCTCCCGCG TCAAGCATAGAATTC-3' (positions 1218 to 1247) (GenBank accession no. NM\_002997); SDC2/sense, 5'-ATGCGGCGCGCGTGGATCCTGCT CACCTT-3' (positions 619 to 647), and SDC2/antisense, 5'-TTACGCA TAAACTCCTTAGTAGGTCCT-T-3' (positions 1195 to 1224) (GenBank accession no. NM\_002998); SDC3/sense, 5'-CCGCCATGAA GCCGGGCGCCCGCACCGTG-3' (positions 50 to 79), and SDC3/antisense, 5'-CACTAGGCATAGAACTCCTCCTGCTTGTC-3' (positions 1356 to 1385) (GenBank accession no. AF248634); SDC4/sense, 5'-ATGGCCCCCGCCGCTCTGTTCCGCGCTGCT-3' (positions 27 to 55), and SDC4/antisense, 5'-TCA CGCGTAGAATCATTGGTGGGGGCTT T-3' (positions 594 to 623) (GenBank accession no. XM\_009530); GPC1/sense, 5'-ATGGAGCTCCGGGCCCCGAGGCTGGTGGCTG-3' (positions 222 to 251), and GPC1/antisense, 5'-TTACCGCCACCGGGGCTT GGCTACTGTAAG-3' (positions 1869 to 1898) (GenBank accession no. NM\_002081). The initiation codons (ATG) and termination codons (TCA, TTA, and CTA, corresponding to TGA, TAA, and TAG, respectively, in the sense frame) are underlined. PCR was performed using LA *Taq* polymerase (Takara Shuzo) as follows: 1 cycle at 94°C for 1.5 min; 35 cycles of 98°C for 20 s, 50°C for 20 s, and 68°C for 3 to 5 min; and a final extension at 68°C for 3 to 5 min. As a control for confirming the integrity and amount of mRNA in each sample, a GAPDH mRNA was amplified with a primer set (GAPDH-F, 5'-TGAAGGTCGGAGTCAACGGATTG GT-3', and GAPDH-R, 5'-CATGTGGCCATGAGGTCCACCAC-3') (GenBank accession no. M17851).

**Establishment of cells expressing SDC1, SDC2, SDC3, SDC4, or GPC1.** The complete open reading frame (ORF) sequences of the human SDC1, SDC2, SDC3, SDC4, and GPC1 genes were obtained by PCR amplification of DNA samples from the pMXpuro/U251MG cDNA library or U251MG cDNA as a template. PCR products were cloned into the retroviral expression vector plasmid pMXpuro or pCXbsr (1). K4R cells were inoculated with retrovirus vector produced by Plat-E or by Phoenix-A cells transfected with the pMXpuro or pCXbsr plasmid containing the ORF sequence for the SDC1, SDC2, SDC3, SDC4, or GPC1 gene. The cells transduced with these vectors were selected by culture in medium containing puromycin at 1  $\mu\text{g}/\text{ml}$  or blasticidin S at 10  $\mu\text{g}/\text{ml}$  for 1 to 2 weeks. The cell lines thus established were named K4R/SDC1, K4R/SDC2, K4R/SDC3, K4R/SDC4, and K4R/GPC1, respectively. Cell lines transduced with pMXpuro or pCXbsr vector alone, namely, K4R/pMX and K4R/pCX, were established as controls. K4R/SDC1 cell clones were obtained by limiting dilution, and clonal cells were assessed for their susceptibilities to VSV $\Delta\text{G}^*$ (HTLV-1).

**Detection of cell-free HTLV-1 infection.** Cell-free HTLV-1 produced by 8C/HTLV-1 cells was prepared as described previously (15, 63). Target cells ( $10^5$  cells/300  $\mu\text{l}$ ) were inoculated with 100  $\mu\text{l}$  of cell-free HTLV-1, which had been treated for 10 min with or without anti-HTLV-1 serum (1%) on ice, and then incubated for 24 h at 37°C in a CO<sub>2</sub> incubator. DNAs of target cells were isolated using a Wizard DNA purification kit (Promega, Madison, WI) and dissolved in 50  $\mu\text{l}$  of Tris-EDTA buffer, and 2  $\mu\text{l}$  was used as the template for qPCR as described above. qPCR was carried out to quantify the HTLV-1 proviral DNA synthesis level using the HTLV-1 pX-specific primers designated pX-F (5'-CCCACTTCCCAGGGTTTGACAGAG-3'; positions 7325 to 7349) and pX-R (5'-CTGTAGAGCTGAGCCGATAACGCG-3'; positions 7504 to 7577) (GenBank accession no. J02029), giving an amplified fragment which was a 203-bp sequence of HTLV-1 pX. qPCR mixtures were preincubated at 95°C for 10 min, followed by 40 to 50 cycles of 95°C for 30 s, 65°C for 30 s, and 72°C for 30 s. As a control for confirming the integrity and amount of DNA in each sample, a human  $\beta$ -globin gene was amplified with a primer set (PCO3, 5'-ACACAAGTGTGTTCACTAGC-3', and PCO4, 5'-CAACTTCATCCACGTTACAC-3') (52).  $\beta$ -Globin gene amplifications were performed at an annealing temperature of 55°C, and all other conditions were the same as described above.

**Syncytium assay.** To investigate the effect of HSPG for syncytium formation, HTLV-1 producing MT-2 cells were cocultured with target cells. Molt-4 cells were used as a positive control T-cell line. Two days after, cells were fixed with 2.5% paraformaldehyde, and the number of syncytia (more than two cell diameters) was counted.

**Treatment of cells with heparitinase I and heparinase.** Heparitinase I and heparinase (Seikagaku Kogyo, Tokyo, Japan) were serially diluted with phosphate-buffered saline (PBS). Serially diluted heparitinase I and heparinase were diluted 10-fold with Opti-MEM I reduced-serum medium (Gibco BRL). Cells were incubated with diluted heparitinase I- or PBS-containing Opti-MEM at 37°C for 1 h.

**Flow-cytometric analysis.** To examine the cell surface expression of GLUT1 and HSPG,  $6 \times 10^5$  cells per sample were prepared for flow-cytometric analysis. Adherent cells were detached from tissue culture dishes using Versene (0.2% EDTA in PBS). The cells were then suspended in 30  $\mu\text{l}$  of PBS containing 3% bovine serum albumin (BSA) and 0.1% sodium azide (PBS-BSA-NaN<sub>3</sub>) and incubated on ice for 30 to 40 min with 1  $\mu\text{g}$  of anti-GLUT1 mouse MAb, clone 202915 (R&D Systems), 2  $\mu\text{g}$  of anti-GLUT1 (N-20) goat polyclonal antibody (PAb) (Santa Cruz), 1.2  $\mu\text{g}$  of anti-SDC1 core protein mouse MAb, clone B-B4 (Immunotech, Marseille, France), or 0.3  $\mu\text{g}$  of anti-HS mouse MAb clone F58-10E4 (Seikagaku Kogyo Co. Ltd., Tokyo, Japan). The cells were washed with PBS containing 1% FBS and 0.1% sodium azide (PBS-FBS-NaN<sub>3</sub>), suspended in 30 to 40  $\mu\text{l}$  of PBS-BSA-NaN<sub>3</sub> containing fluorescein isothiocyanate (FITC)-conjugated rabbit anti-mouse immunoglobulin (IgG) (1:30; MBL, Nagoya, Japan) or FITC-conjugated rabbit anti-goat IgG (1:30; ICN/Cappel, Costa Mesa, CA) secondary Ab, and incubated on ice for 30

to 40 min. The cells were washed with PBS-FBS-NaN<sub>3</sub> and suspended in 300 to 600  $\mu\text{l}$  of PBS containing 1% paraformaldehyde, and then flow-cytometric analysis (FCM) was performed using a flow cytometer, model Cyto ACE-100 (Jasco, Tokyo, Japan). As a control, the cells were treated with the secondary Ab alone and were subjected to FCM. To detect the HS neo-epitopes ( $\Delta\text{HS}$ ) generated at the terminal stubs of the HS by digestion with heparitinase I,  $1 \times 10^6$  to  $2 \times 10^6$  cells were resuspended in 100 to 200  $\mu\text{l}$  of Opti-MEM reduced-serum medium (Gibco BRL) and incubated with heparitinase I (10 mU/ml) (Seikagaku Kogyo Co. Ltd.) for 1 h at 37°C. Six hundred thousand cells were then washed with PBS, suspended in 30  $\mu\text{l}$  of PBS-BSA-NaN<sub>3</sub>, and stained with 0.3  $\mu\text{g}$  of anti- $\Delta$ -HS mouse MAb, clone F69-3G10 (10  $\mu\text{g}/\text{ml}$ ) (Seikagaku Kogyo Co. Ltd.), as described above.

## RESULTS

**Preparation of VSV pseudotypes bearing HTLV-1 Env proteins.** VSV $\Delta\text{G}^*$ -G, a recombinant VSV carrying a GFP reporter gene, efficiently infected C8166 human T cells, as indicated by the GFP-positive cells detected by fluorescence microscopy (Fig. 1A). This infectivity was almost completely inhibited by the pretreatment of VSV $\Delta\text{G}^*$ -G with anti-VSV serum. VSV $\Delta\text{G}^*$ -G was then inoculated into 8C/HTLV-1<sub>2M</sub> or 8C/HTLV-1<sub>MEL5</sub> cells to produce the VSV $\Delta\text{G}^*$  pseudotypes, VSV $\Delta\text{G}^*$ (HTLV-1<sub>2M</sub>), or VSV $\Delta\text{G}^*$ (HTLV-1<sub>MEL5</sub>), respectively. VSV $\Delta\text{G}^*$ (HTLV-1<sub>2M</sub>) and VSV $\Delta\text{G}^*$ (HTLV-1<sub>MEL5</sub>) were capable of infecting approximately 20 to 30% of C8166 human cells even after pretreatment with anti-VSV serum (Fig. 1A), and the infectivity was drastically reduced by pretreatment of the pseudotypes with a MAb specific for the HTLV-1 Env gp46 (data not shown) or with 0.2% anti-HTLV-1 human serum (Fig. 1A) but not with anti-BLV antisera (data not shown). We also confirmed that VSV $\Delta\text{G}^*$ -G infectivity was not significantly affected by treatment with anti-HTLV-1 antisera or anti-BLV antisera (data not shown). As expected from viral interference, VSV $\Delta\text{G}^*$ (HTLV-1) was nearly undetectable in cell lines expressing HTLV-1 Env (MT-2 and C91/PL) (Fig. 1B). These data indicated that infectious pseudotypes bearing HTLV-1 Env could be produced.

**Susceptibilities of different human cell lines to HTLV-1 pseudotypes and their expression levels of GLUT1, NRP-1, and cell surface HS chains.** We investigated the susceptibility of several human cell lines to the HTLV-1 pseudotype and VSV $\Delta\text{G}^*$ -G, including 293T, C8166, HOS, Molt-4, U251MG, and the CD4-transduced K562 cell clone K4R. These cells were inoculated with VSV $\Delta\text{G}^*$ (HTLV-1<sub>MEL5</sub>) or VSV $\Delta\text{G}^*$ G, and GFP expression was monitored the next day (Fig. 1B). These cell lines varied in permissiveness to the HTLV-1 pseudotype. In particular, U251MG cells were approximately 1,600-fold more susceptible than K4R cells (Fig. 1B). This U251MG cell line has been shown to be highly susceptible to HTLV-1 virions in a cell-free infection system (15). In contrast, the susceptibility of U251MG cells to VSV $\Delta\text{G}^*$ -G was only 4-fold higher than that of K4R cells (Fig. 1B).

FCM revealed that the levels of cell surface GLUT1 expression detected with anti-GLUT1 mouse MAb ( $r = 0.52$ ,  $P = 0.29$ ) and anti-GLUT1 goat Pab ( $r = 0.01$ ,  $P = 0.34$ ) were not significantly correlated with susceptibility to the HTLV-1 pseudotype among these cell lines (Fig. 1C). Although we observed the highest reactivity of anti-GLUT1 mouse MAb to the U251MG cells and the lowest reactivity to the K4R cells, Kinet et al. (30a) reported that this MAb does not detect endogenous GLUT1 but rather interacts with a cell surface protein which is associated with GLUT1 over-expression in transformed cell lines. In addition, the cell surface HS expression level, determined by FCM using the MAb F58-

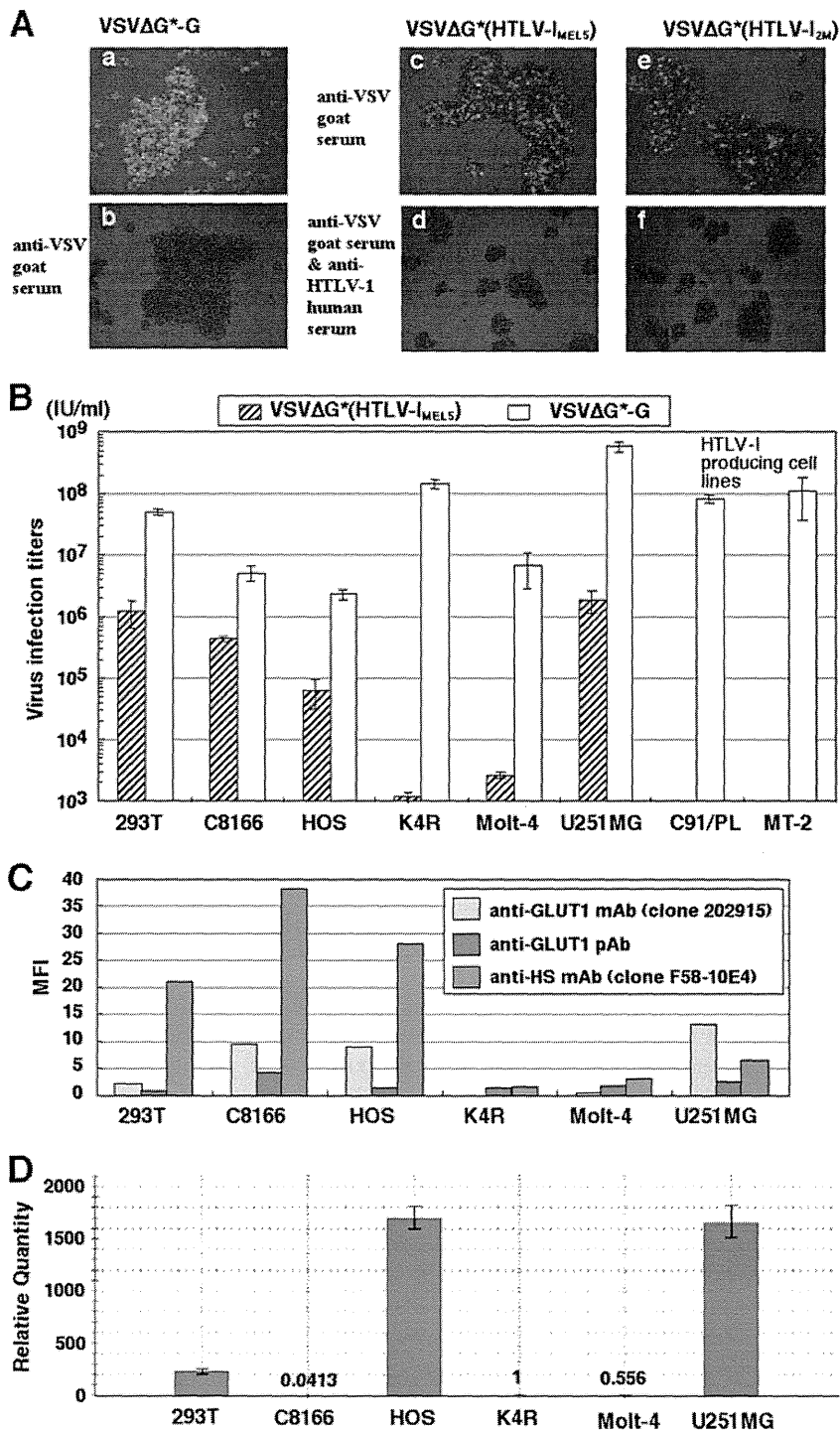


**FIG 1** Susceptibility of cell lines to VSVΔG\* pseudotypes bearing the HTLV-1 Env protein. (A) C8166 cells were inoculated with VSVΔG\*-G in the absence (a) or presence (b) of anti-VSV goat serum (1%). C8166 cells were also inoculated with VSVΔG\*(HTLV-1<sub>MEL5</sub>) and VSVΔG\*(HTLV-1<sub>2M</sub>) pseudotypes treated with anti-VSV goat serum (5%), in the absence (c and e) or presence (d and f) of anti-HTLV-1 human serum (0.2%). One day after inoculation, the cells were observed by fluorescence microscopy. (B) Titration of the VSVΔG\*(HTLV-1<sub>MEL5</sub>) and VSVΔG\*-G using various human cell lines. VSVΔG\*(HTLV-1<sub>MEL5</sub>) treated with anti-VSV goat serum (see Materials and Methods) and VSVΔG\*-G were serially diluted 10-fold, and cells were inoculated to determine the respective titers. Each titer was calculated from the number of GFP-positive cells in endpoint dilutions. (C) Expression of GLUT1 and HS chains on the surface of various cell lines. Expression of GLUT1 and HS chains in human cell lines was examined by FCM. Cells were stained with anti-GLUT1 mouse MAb 202915, anti-HS mouse MAb F58-10E4, or anti-GLUT1 goat PAb and then stained with an FITC-conjugated rabbit anti-mouse IgG or an FITC-conjugated rabbit anti-goat IgG secondary Ab. Mean fluorescent intensities detected by the anti-GLUT1 MAb, the anti-GLUT1 PAb, and the anti-HS mouse MAb were determined by subtracting the MFI of the negative controls (secondary Ab alone). (D) Relative mRNA expression levels of NRP-1 in various cell lines were measured by real-time RT-PCR and the values were normalized to expression levels of GAPDH mRNA.

10E4, which reacts with epitopes containing N-sulfated glucosamine residues present in many types of HS (4, 65), did not significantly correlate with susceptibility to the HTLV-1 pseudotype (Fig. 1C). Moreover, the mRNA expression levels of NRP-1 did not correlate with the susceptibilities to the HTLV-1 pseudotype in six different cell lines ( $r = 0.41$ ,  $P = 0.42$ ) (Fig. 1D). Thus, the range in susceptibility to HTLV-1 among these cell lines could not be explained by the respective expression levels of GLUT1, cell surface HS, or NRP-1 independently. Although another explanation in which the expression balance of GLUT-1, HS, and NRP-1 affects the HTLV-1 susceptibilities would be possible, we adopted a working hypothesis that an unknown cellular factor may also be involved.

**Identification of molecules responsible for the increased susceptibility to HTLV-1 pseudotype.** To investigate cellular factors other than GLUT-1, HS, and NRP-1 affecting the HTLV-1 susceptibility, we attempted to identify the responsible factor from U251MG cells, which were permissive to the HTLV-1 pseudotype. We generated a pMX vector-based retroviral expression cDNA library from U251MG cells and transduced the library into K4R cells, which were least HTLV-1 susceptible. cDNA library-expressing K4R cells were seeded into 96-well plates (20 to 40 cells/well), and cultured for 2 weeks. Cells were then screened for their susceptibilities to VSV $\Delta$ G\*(HTLV-1<sub>MEL5</sub>). Eighty-three of 5,088 wells showed an increased frequency of GFP-positive cells in the first round of screening and were then subjected to a second round of screening. In that screening, two wells, designated w16 and w40, showed a >3-fold increase in GFP-positive cells compared to other wells, and those cells were subsequently cloned. Cell clones derived from each well, K4R/cDNA-w16-c and K4R/cDNA-w40-c, demonstrated 40-fold-higher susceptibilities to the HTLV-1 pseudotype than the parental K4R cells (Fig. 2A and B).

To identify the molecule(s) responsible for the increased susceptibility to the HTLV-1 pseudotype, genomic DNA was extracted from K4R/cDNA-w16-c and K4R/cDNA-w40-c and subjected to PCR amplification using pMX vector-specific primers. Two fragments of 1.3 and 2.0 kb were amplified from w16-c and w40-c clones, respectively (Fig. 2C), and subsequently cloned into a pCR2.1 vector to determine their nucleotide sequences. Contrary to our expectations, K4R/cDNA-w16-c contained a cDNA corresponding to nt 49 to 1331 of the human SDC1 gene transcript variant 2 (GenBank accession no. NM\_002997), and K4R/cDNA-w40-c contained cDNA corresponding to nt 297 to 2312 of the human SDC2 gene (GenBank accession no. NM\_002998).

The SDC family core proteins have previously been reported to exhibit cell type-specific distributions (5, 9, 30). In addition to SDCs, cell surface HSPGs include GPC (5, 9, 30). We therefore examined the expression levels of several cell surface HSPG core protein mRNAs by RT-PCR and found that each cell line expressed different combinations of HSPG core protein mRNAs (Fig. 2D). The U251MG cell line, which was most susceptible to HTLV-1 pseudotype infection, expressed all four SDC core proteins and GPC-1 mRNAs, whereas the K4R cells, which were least susceptible, expressed only SDC1, SDC4, and GPC1 mRNAs.

To confirm whether the transduction of these HSPG core protein genes was responsible for the increased susceptibility to the HTLV-1 pseudotype, we established K4R cells transduced with SDC1, SDC2, SDC3, SDC4, and GPC1 cDNA, referred to as K4R/SDC1, K4R/SDC2, K4R/SDC3, K4R/SDC4, and K4R/GPC1 cells, respectively. We then examined their susceptibilities to HTLV-1

pseudotypes. All of these transduced cells exhibited a >20-fold increase in susceptibility to both VSV $\Delta$ G\*(HTLV-1<sub>MEL5</sub>) and VSV $\Delta$ G\*(HTLV-1<sub>2M</sub>) pseudotypes compared to the transduced control cells (K4R/pMX) (Fig. 2E). In contrast, susceptibilities of these transduced cells to both VSV $\Delta$ G\*-G and VSV $\Delta$ G\*(BLV) pseudotypes were within 2-fold of the transduction control cells (K4R/pMX) (Fig. 2E).

Next we examined the susceptibilities of K4R/SDC1, K4R/SDC2, K4R/SDC3, K4R/SDC4, and K4R/GPC1 cells to cell-free wild-type HTLV-1. These cells were inoculated with HTLV-1<sub>2M</sub>, and the proviral DNA was detected 24 h postinfection by qPCR. Consistent with the results obtained with HTLV-1 pseudotypes (Fig. 2E), the susceptibility of K4R cells to cell-free HTLV-1 was increased markedly by the transduction of HSPG core protein genes (Fig. 2F).

**Expression of HSPG core proteins in K4R cells induces cell aggregation but does not increase cell fusion activity to HTLV-1-producing MT-2 cells.** We observed that K4R cells transduced with HSPG core protein genes formed cell clumps, as shown in Fig. 3A. These cellular aggregations were observed in all species of SDCs and GPC1 (data not shown), indicating that the expression of HSPGs induced cell-cell adhesion. Similar to our observation, HS-dependent cell-cell adhesion has been reported in B lymphoid cell lines and cells transduced with SDC1 (36, 56, 60). To determine whether this increased cell-cell contact mediated by HSPG is related to the fusion activity with an HTLV-1-producing cell line, we conducted a syncytium assay as described in Materials and Methods. We observed syncytia in the coculture of HTLV-1-producing MT-2 cells with both K4R cells (Fig. 3B) and Molt-4 T cells (data not shown). The cell fusion was effectively inhibited by anti-HTLV-1 serum (Fig. 3C). The number of syncytia in the coculture of K4R/SDC1 with MT-2 cells was lower than that in the coculture of MT-2 cells with parental K4R cells or vector-transduced K4R cells (Fig. 3C). These findings indicate that the increased cell-cell adhesion mediated by cell surface expression of HSPGs does not contribute to membrane fusion between target cells and HTLV-1-producing cells.

**Reduced susceptibility to VSV $\Delta$ G\*(HTLV-1) following heparitinase I or heparinase treatment.** K4R cells transduced with HSPG core proteins (SDC1, SDC2, SDC3, SDC4, and GPC1) showed increased cell surface expression of HS, as detected by an anti-HS MAb, F58-10E4 (Fig. 4A). To evaluate the role of HS in the increased susceptibility to the HTLV-1 pseudotype, the transduced cells were treated with the HS-degradative enzyme heparitinase I and the heparin-degradative enzyme heparinase. Almost all of the HS chains detected by the MAb F58-10E4 on K4R/SDC1 cells were trimmed by heparitinase I treatment (Fig. 4B). The susceptibility of the heparitinase I-treated K4R/SDC1 cells was reduced to about one-tenth of that of the untreated cells (Fig. 4C). Although the susceptibilities to the pseudotyped virus were similarly reduced by heparinase treatment (Fig. 4C), most of the HS chains detected by the MAb F58-10E4 remained on the K4R/SDC1 cells (Fig. 4B). These results indicate that HS chains, which remained on the cell surface after heparinase treatment, did not support HTLV-1 infection of K4R/SDC1 cells. In other words, the reduced region of HS chains, which could not be detected by the MAb F58-10E4, played a critical role in increasing the susceptibility to HTLV-1. Heparinase cleaves heparin or highly sulfated heparin-like structural regions of HS chains at the alpha-glucosaminide linkage to 2-O-sulfo-L-iduronic acid, in which



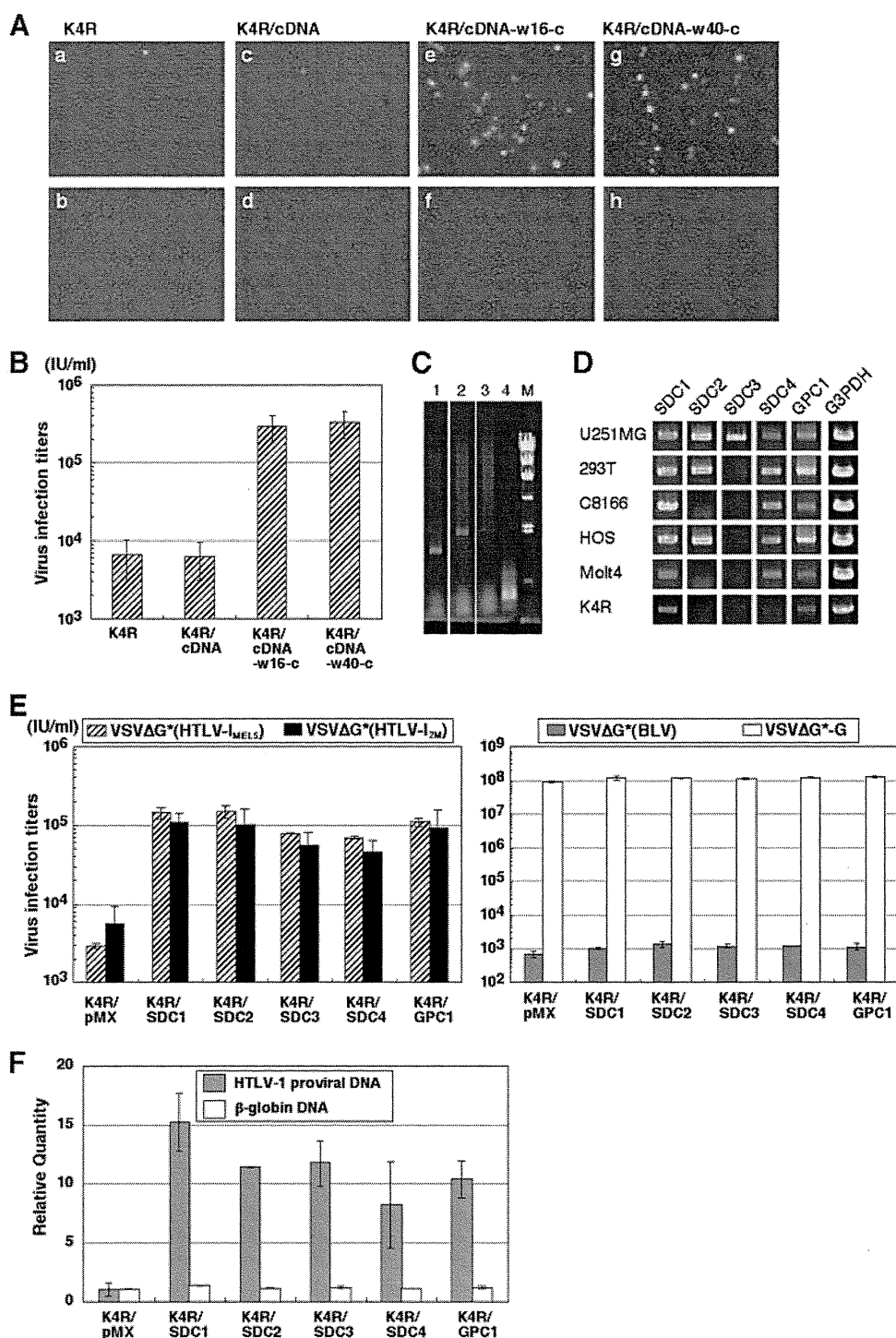


**FIG 2** K4R cell clones transduced with the U251MG cDNA library showed an enhanced susceptibility to the HTLV-1 pseudotypes. (A) Detection of GFP-positive cells inoculated with the VSVΔG\*(HTLV-1<sub>MEL5</sub>). Parental K4R cells (a and b), K4R cells transduced with the U251MG cDNA library (K4R/cDNA cells) (c and d), and two K4R/cDNA cell clones showing increased HTLV-1-susceptibility (K4R/cDNA-w16-c [e and f] and K4R/cDNA-w40-c cells [g and h]) were inoculated with VSVΔG\*(HTLV-1<sub>MEL5</sub>) treated with anti-VSV goat serum (final concentration of 10%) in the absence (a, c, e, and g) or presence (b, d, f, and h) of anti-HTLV-1 serum (final concentration of 0.2%). (B) Enhanced susceptibilities of two K4R/cDNA cell clones to VSVΔG\*(HTLV-1<sub>MEL5</sub>) infection. VSVΔG\*(HTLV-1<sub>MEL5</sub>) infectious titers of each cell calculated from the number of GFP-positive cells in endpoint dilutions are shown. (C) Detection of introduced cDNAs harbored in the K4R/cDNA-w16-c and K4R/cDNA-w40-c cells. Genomic DNA from K4R/cDNA-w16-c, K4R/cDNA-w40-c, and parental K4R cells and pMXpuro plasmid DNA were subjected to PCR using specific primers for the pMXpuro vector to detect transduced cDNA. Lanes: 1, K4R/cDNA-w16-c; 2, K4R/cDNA-w40-c; 3, parental K4R; 4, pMXpuro plasmid DNA; M, molecular size marker (A DNA Hind III digest). (D) Expressions of SDCs and GPC1 in various human cell lines. Cellular RNA extracted from human cell lines for the expression of SDC1, SDC2, SDC3, SDC4, and GPC1 genes was amplified by RT-PCR. GAPDH mRNA was amplified as a control. (E) Enhanced susceptibilities of K4R cells transduced with HSPG core protein genes to the HTLV-1 pseudotypes. Cells were inoculated with serially diluted VSVΔG\*(HTLV-1<sub>MEL5</sub>), VSVΔG\*(HTLV-1<sub>2M</sub>), and VSVΔG\*(BLV) pseudotypes treated with anti-VSV goat serum (see Materials and Methods) or VSVΔG\*-G. Three independent experiments were done, and the data are from one representative experiment of the three. (F) Enhanced susceptibilities of K4R cells transduced with HSPG core protein genes to the cell-free HTLV-1. Cells were inoculated with cell-free wild-type HTLV-1<sub>2M</sub> and the formation of HTLV-1 DNA was monitored by real-time PCR using the pX region primer 24 h postinfection. β-Globin DNA in each sample was amplified as a control. Three independent experiments were done, and the data are from one representative experiment of the three.

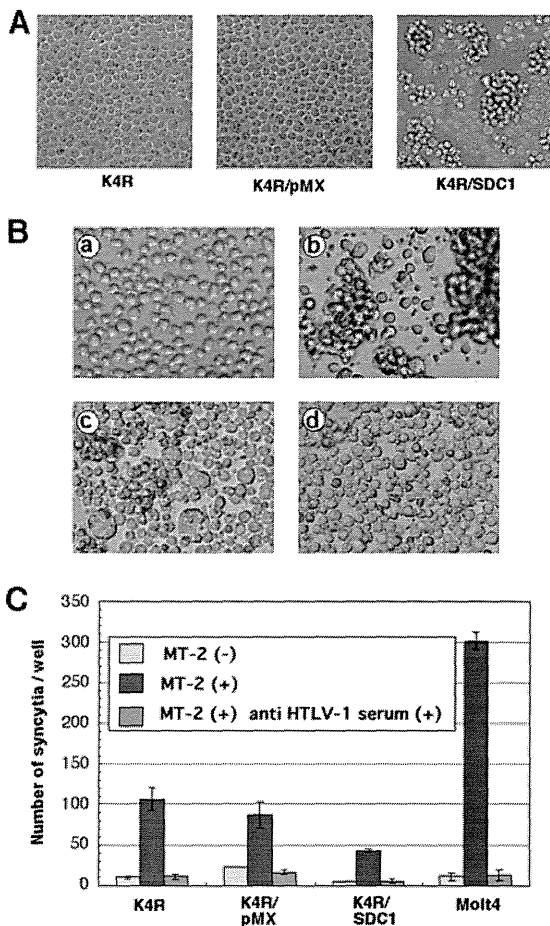


**FIG 3** Expression of HSPG core proteins induces cell aggregation but does not increase cell fusion activity with HTLV-1-producing MT-2 cells. Cell surface expression of HSPG core protein does not increase cell fusion activity when the protein is incubated with HTLV-1-producing cells. The expression of HSPG core protein (A) K4R cells transduced with the HSPG core protein gene frequently showed cell clumps. Under normal culture conditions, K4R/SDC1 cells but not parental or vector-transduced K4R cells showed the formation of aggregates. (B) Syncytium formation in K4R cells cocultured with MT-2 cells. K4R cells (a), MT-2 cells (b), and cocultured K4R and MT-2 cells in the absence (c) or presence (d) of anti-HTLV-1 serum (final concentration at 1%) were fixed 4 days after coculture. (C) No augmentation of syncytium formation in K4R cells by overexpression of SDC1 was observed. The syncytium assay was conducted by coculturing  $2 \times 10^4$  target cells (K4R, K4R/pMX, K4R/SDC1, and Molt-4 cells with MT-2 cells [ $5 \times 10^3$ ] in a 96-well plate at 37°C for 2 days in the absence or presence of anti-HTLV-1 serum [final concentration, 0.5%]). The number of syncytia was counted as the number of large cells whose diameter was greater than twice that of normal cells ( $1.5 \pm 0.5 \mu\text{m}$ ). Two independent experiments were done, and the data are from one representative experiment of the two.

2-deoxy-2-sulfoamino-(6-O-sulfo)-D-glucose participates (37). Therefore, there are two possible explanations for this phenomenon: (i) highly sulfated heparin-like structure regions of HS chains digested by heparinase exist on only a few HS chains, or (ii) such regions exist on only the terminal region of HS chains, which is distant from the core protein. In support of the latter explanation, it was recently reported that there are highly sulfated structures in the distal ends of HS chains (61, 68). Thus, we posited that HTLV-1 interacted with these heparinase-sensitive heparin-like regions, which are located at the distal, nonreducing end of HS in K4R/SDC1 cells.

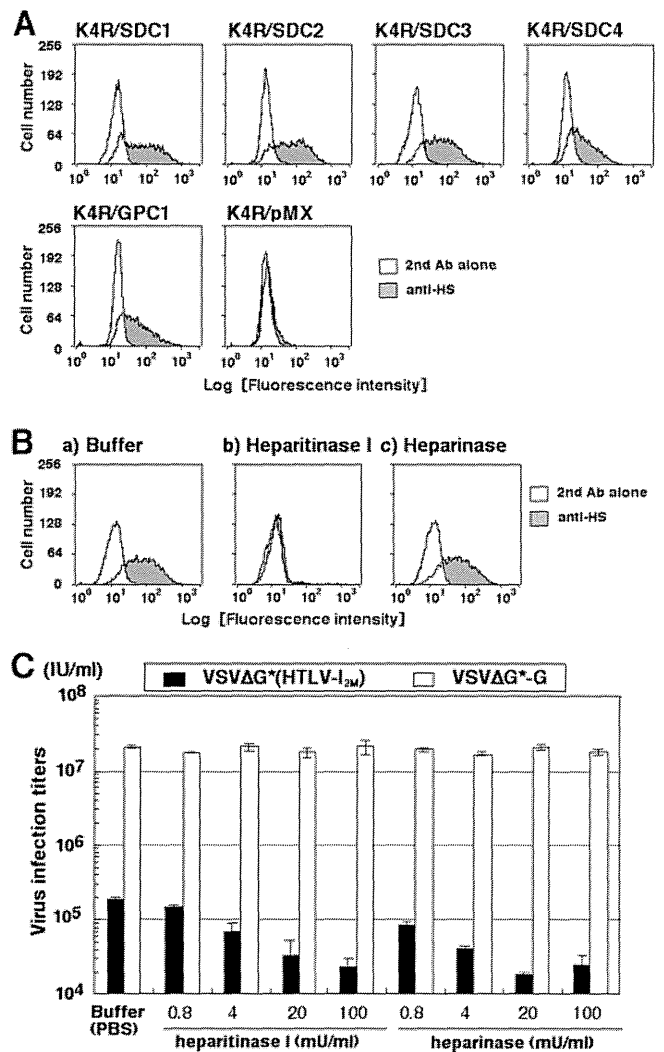


**FIG 4** Cell surface expression of HS detected by anti-HS MAb F58-10E4 did not affect HTLV-1 pseudotype infection. (A) Cell surface HS chains in K4R cells transduced with the SDC1, SDC2, SDC3, SDC4, or GPC1 core protein gene were stained with F58-10E4, treated with FITC-conjugated anti-mouse IgG, and analyzed by FCM. (B) Cell surface HS was examined by treating cells with buffer, heparitinase I (10 mU/ml), or heparinase (20 mU/ml) were stained with F58-10E4 and FITC-conjugated anti-mouse IgG and then analyzed by FCM. (C) K4R/SDC1 cells treated with heparitinase I or heparinase at the indicated concentrations were seeded into 96-well plates ( $4 \times 10^4$  cells/well) before inoculation with VSVΔG\*(HTLV-1<sub>2M</sub>) or VSVΔG\*-G. One day after inoculation, the GFP-positive cells were counted under a fluorescence microscope. Three independent experiments were done, and the data are from one representative experiment of the three.

**Formula for expressing the relationship between cell surface expression of HS and HTLV-1 susceptibility.** To examine how the expressed form of the HS chains influences the susceptibilities of the cells to HTLV-1 infection, we established several K4R/SDC1 cell clones and examined their susceptibilities to HTLV-1 pseudotypes in relation to HS chain contents. To define the contents of the HS chains on the cells, the total amount and the number of HS chains were detected separately by FCM using two different MABs, F58-10E4 and F69-3G10, respectively.

The total amount of expressed HS chains (the net level of HS per cell) was assessed by using the MAB F58-10E4, which is expected

TABLE 1 Susceptibility of K4R/SDC1 cell clones to the HTLV-1 pseudotype and their HS chain content

| Expt <sup>a</sup>     | Clone               | Infectious titer of pseudotype virus (IU/ml) | MFI determined by FCM |                     |  | MFI <sub>3G10</sub> × (MFI <sub>10E4</sub> /MFI <sub>3G10</sub> ) <sup>-1</sup> |
|-----------------------|---------------------|--|-----------------------|---------------------|--|---|
|                       |                     |  | MFI <sub>10E4</sub>   | MFI <sub>3G10</sub> | MFI <sub>10E4</sub> /MFI <sub>3G10</sub> |   |
| 1                     | K4R/SDC1 (parental) | 310,000                                      | 18                    | 204                 | 0.088                                    | 2,312   |
| 3                     | K4R/SDC1 (parental) | 170,000                                      | 53                    | 256                 | 0.207                                    | 1,237   |
| 1                     | Clone 1             | 640,000                                      | 29                    | 362                 | 0.080                                    | 4,519   |
| 2                     | Clone 1             | 560,000                                      | 28                    | 401                 | 0.070                                    | 5,743   |
| 4                     | Clone 1             | 180,000                                      | 78                    | 227                 | 0.344                                    | 661   |
| 1                     | Clone 2             | 300,000                                      | 39                    | 429                 | 0.091                                    | 4,719   |
| 3                     | Clone 2             | 81,000                                       | 48                    | 135                 | 0.356                                    | 380   |
| 1                     | Clone 3             | 480,000                                      | 21                    | 396                 | 0.053                                    | 7,467   |
| 3                     | Clone 3             | 180,000                                      | 39                    | 226                 | 0.173                                    | 1,310   |
| 3                     | Clone 4             | 62,000                                       | 37                    | 251                 | 0.147                                    | 1,703   |
| 4                     | Clone 4             | 170,000                                      | 72                    | 401                 | 0.180                                    | 2,233   |
| 2                     | Clone 5             | 350,000                                      | 25                    | 322                 | 0.078                                    | 4,147   |
| 3                     | Clone 5             | 270,000                                      | 69                    | 258                 | 0.267                                    | 965   |
| 4                     | Clone 5             | 120,000                                      | 59                    | 159                 | 0.371                                    | 428   |
| <i>r</i> <sup>b</sup> |                     |  | -0.562                | 0.650               | -0.690                                   | 0.816   |
| <i>P</i>              |                     |  | 0.036                 | 0.012               | 0.0062                                   | 0.00037   |

<sup>a</sup> Experiments 1 to 4 were carried out with the same stock of VSVΔG\*(HTLV-1<sub>2M</sub>).

<sup>b</sup> Coefficient of correlation relative to the infectious titer of the HTLV-1 pseudotype.

to trace the mass of HS chains (4), and the results were expressed as the mean fluorescence intensity (MFI<sub>10E4</sub>). Initially, we noticed that the cell surface expression of HS in each clone and parental K4R/SDC1 cells fluctuated depending on the test occasion (Table 1). Given that HS expression has been reported to vary in Molt-4 cells in relation to the cell growth (27), the observed fluctuation of HS expression in each clone might reflect the subtle differences in culture conditions. We repeated the experiments at least twice for each clone and found that the MFI<sub>10E4</sub> of the K4R/SDC1 clones moderately and negatively correlated with susceptibilities to VSVΔG\*(HTLV-1<sub>2M</sub>) ( $r = -0.562$ ;  $P = 0.036$ ) (Table 1).

Next, the number of HS chains was assessed by using MAB F69-3G10, which specifically recognizes the HS neo-epitopes (ΔHS) generated at the terminal stubs of HS in heparitinase I-treated cells. Since HS chains are unbranched disaccharide polymers, and heparitinase I cuts the α-N-acetyl-D-glucosaminidic linkage in HS chains of HSPGs, one ΔHS epitope was generated at the stub of each HS chain (43). Thus, F69-3G10 staining was the representative of the number of HS chains expressed on the cell surface. We observed a moderate correlation between the number of HS chains deduced by MFI<sub>3G10</sub> on the heparitinase I-treated K4R/SDC1 cell clones and the susceptibilities to VSVΔG\*(HTLV-1<sub>2M</sub>) ( $r = 0.650$ ;  $P = 0.012$ ) (Table 1). We assumed that the value we calculated by dividing the total mass of HS chains expressed (MFI<sub>10E4</sub>) by the total number of HS chains (MFI<sub>3G10</sub>) would reflect the mean length of the HS chains on the cells. The value of MFI<sub>10E4</sub>/MFI<sub>3G10</sub> in K4R/SDC1 clones showed a significant negative correlation with the susceptibilities to VSVΔG\*(HTLV-1<sub>2M</sub>) ( $r = -0.690$ ;  $P < 0.01$ ) (Table 1), suggesting that short HS chains might contribute to the more efficient entry of the HTLV-1 pseudotype. Furthermore, an index for short HS chains could be derived by the following formula: number of HS chains (MFI<sub>3G10</sub>) × reciprocal length of HS chains (MFI<sub>10E4</sub>/MFI<sub>3G10</sub>). The value of MFI<sub>3G10</sub> × (MFI<sub>10E4</sub>/MFI<sub>3G10</sub>)<sup>-1</sup> in K4R/SDC1 clones significantly correlated with the susceptibility to the HTLV-1 pseudotype ( $r = 0.816$ ;  $P < 0.001$ ) (Table 1 and Fig. 5A). Next, we examined whether the susceptibility to the HTLV-1 pseudotype in

8 different human cell lines correlated with the following parameters: number of SDC1 molecules (MFI<sub>B4</sub>), amount of HS chains, number of HS chains, mean length of HS chains, and short-HS-chain index, deduced by the following formula: MFI<sub>3G10</sub> × (MFI<sub>10E4</sub>/MFI<sub>3G10</sub>)<sup>-1</sup>. We found that the values of MFI<sub>B4</sub>, MFI<sub>10E4</sub>, MFI<sub>3G10</sub> and MFI<sub>10E4</sub>/MFI<sub>3G10</sub> for each cell line did not

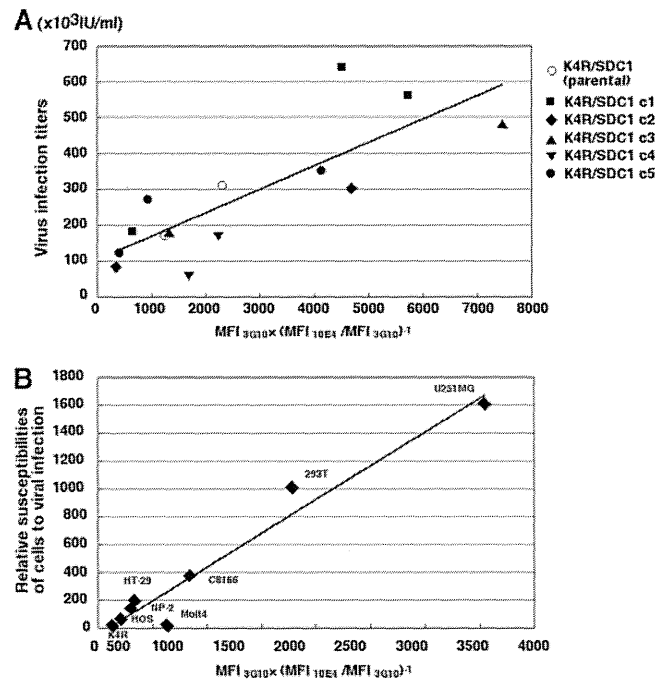


FIG 5 The linear relationship between the susceptibilities to HTLV-1 pseudotype infection and short HS chain index [MFI<sub>ΔHS</sub> × (MFI<sub>HS</sub>/MFI<sub>ΔHS</sub>)<sup>-1</sup>]. (A) Susceptibilities of K4R/SDC1 parental cells and derived clones to the VSVΔG\*(HTLV-1<sub>2M</sub>) were plotted against short-HS-chain indexes (Table 1). (B) Relative susceptibilities of human cell lines to the VSVΔG\*(HTLV-1<sub>MEL5</sub>) were plotted against short-HS-chain indexes (Table 2). The lines show correlation.

TABLE 2 Relative susceptibility of human cell lines to the HTLV-1 pseudotype and their HS chain content

| Cell line             | Relative susceptibility to HTLV-1 pseudotype <sup>a</sup> | MFI determined by FCM |                     |                     |  | $MFI_{3G10} \times (MFI_{10E4}/MFI_{3G10})^{-1}$ |
|-----------------------|---|-----------------------|---------------------|---------------------|--|--|
|                       |   | MFI <sub>B4</sub>     | MFI <sub>10E4</sub> | MFI <sub>3G10</sub> | MFI <sub>10E4</sub> /MFI <sub>3G10</sub> |  |
| U251MG                | 1,600   | 150                   | 6.5                 | 152                 | 0.043                                    | 3,554  |
| 293T                  | 1,000   | 25                    | 21                  | 194                 | 0.108                                    | 1792   |
| C8166                 | 370   | 210                   | 38                  | 180                 | 0.211                                    | 853  |
| HT-29                 | 190   | 157                   | 167                 | 241                 | 0.693                                    | 348  |
| NP-2                  | 130   | 28                    | 77                  | 153                 | 0.503                                    | 304  |
| HOS                   | 53  | 26                    | 28                  | 78                  | 0.359                                    | 217  |
| Molt4                 | 2.3   | 6                     | 3                   | 44                  | 0.068                                    | 645  |
| K4R                   | 1.0   | 0.1                   | 1.5                 | 14                  | 0.107                                    | 131  |
| <i>r</i> <sup>b</sup> |   | 0.37                  | -0.24               | 0.41                | -0.42                                    | 0.98   |
| <i>P</i>              |   | 0.36                  | 0.57                | 0.31                | 0.30                                     | <0.0001  |

<sup>a</sup> Relative susceptibilities of cells to VSVΔG\*(HTLV-1<sub>MEL3</sub>).

<sup>b</sup> Coefficient of correlation relative to the relative susceptibility of the HTLV-1 pseudotype.

significantly correlate with susceptibility to the HTLV-1 pseudotype, whereas the value of  $MFI_{3G10} \times (MFI_{10E4}/MFI_{3G10})^{-1}$  did significantly correlate ( $r = 0.98$ ,  $P < 0.0001$ ) (Table 2 and Fig. 5B). These results suggest that the amount of HS chains or the number of HS chains alone did not determine the cellular susceptibility to the HTLV-1 pseudotype.

## DISCUSSION

In the present study, we first examined the susceptibilities of different cell types by using highly infectious VSV pseudotypes harboring the Env protein of HTLV-1 and found that there was no significant correlation between the cellular susceptibility to HTLV-1 infection and the expression of GLUT1, HS, or NRP-1, which have been identified as the main cellular factors for binding and entry of HTLV-1 (13, 39, 48). To investigate whether other cellular factors were responsible for HTLV-1 susceptibility, we carried out expression cloning to identify cellular molecules that are associated with HTLV-1 susceptibility, other than GLUT1, HSPG, and NRP-1. Consequently, the cell surface HSPG core proteins SDC1 and SDC2 were identified as molecules that are responsible for HTLV-1 susceptibility.

Enhanced susceptibilities of K562 cells transduced with HSPG core genes were also previously observed in human immunodeficiency virus type 1 and human papillomavirus type 11 (54, 57). In these experiments, transduction of SDC1 is more effective in increasing the susceptibility of cells to viral infection than that of GPC1, and Shafti-Keramat and colleagues observed a correlation between HS expression and the relative expression level of HSPGs (54, 57). Although we observed an enhanced susceptibility of K4R cells transduced with HSPG core genes to cell-free HTLV-1 infection, the correlation between various expression levels of cell surface HS and susceptibilities to HTLV-1 among other cell lines (Fig. 1C) remained unclear. We believe that the discrepancy of the HTLV-1 cell tropism may be explained in the context of HS expression, since there is considerable variation in the structure of HS on the cell surface, including differences in sugar components, patterns of sulfation and HS chain length (7, 25, 33). As a clue to address this issue, we found that K4R/SDC1 cells treated with the heparin-degradative enzyme heparinase showed reduced HTLV-1 susceptibility without significantly alteration of the expression of HS chains. This finding indicated that most of the HS chains detected by MAb F58-10E4 were not responsible for HTLV-1 susceptibility.

To investigate in-depth how HS expression affects HTLV-1 susceptibility, we established the K4R/SDC1 clones expressing HS chains

at various levels and examined their susceptibilities to the HTLV-1 pseudotype. Our findings suggest that the number of HS chains, but not their mass, is one of the factors affecting HTLV-1 susceptibility. To clarify why the mass of HS chains did not affect the susceptibility of HTLV-1 infection, we investigated the HS chain length as one of the parameters reflecting the amount of HS. However, it was difficult to accurately determine the HS chain length in various compositions of HS chains; therefore, we calculated the value of the mean length of HS chains by dividing the mass by the number of HS chains. This value, represented by  $MFI_{10E4}/MFI_{3G10}$ , was negatively correlated with the HTLV-1 susceptibility of each K4R/SDC1 cell clone. Next, we considered that shorter HS chains might contribute to the efficiency of HTLV-1 entry, and that the number of shorter HS chains may be important for HTLV-1 susceptibility. The value obtained by multiplying the number of HS chains ( $MFI_{3G10}$ ) by the inverse mean length of HS chains ( $MFI_{10E4}/MFI_{3G10}$ ) significantly correlated with the HTLV-1 susceptibility in not only K4R/SDC1 clones but also in various human cell lines. This short-HS-chain index, given by  $MFI_{3G10} \times (MFI_{10E4}/MFI_{3G10})^{-1}$ , will increase when the cells express larger numbers of shorter HS chains, whereas the value will decrease when the cells express fewer and longer HS chains. This observation indicates that human cell lines expressing not only larger numbers of HS chains but also shorter lengths of HS chains were more susceptible to HTLV-1 infection.

Although we determined only the relative length in this study, the average length of HS chains has been reported to be between 50 and 200 disaccharide repeats, corresponding to 40 to 160 nm in length (64). These HS chains are assumed to adopt extended structures when they are in aqueous solution because their extensive sulfation makes them hydrophilic (23). From this point of view, our findings provide a possible model to explain the difference in HTLV-1 susceptibility between cells expressing different-length HS chains. HTLV-1 particles may get closer to the target cell surface when they bind to heparin-like regions in short HS chains (Fig. 6). In other words, the high expression level of HS chains that are detected by the MAb F58-10E4 impedes the entry of HTLV-1. Recently, Jastrebova and colleagues reported that contiguous sulfated domains were the most abundant in the shortest HS chains and that short HS chains promoted fibroblast growth factor 2 (FGF2) cellular signaling more efficiently than longer HS chains by the formation of ternary complexes (FGF2-HS-FGF receptor) (25). It has been reported that HSPGs and NRP-1 function cooperatively during the initial binding of HTLV-1

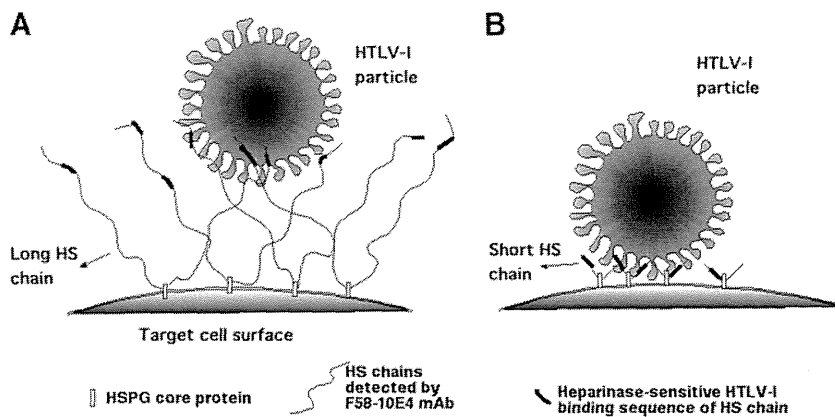


FIG 6 Hypothetical model showing interactions of HTLV-1 particles and cell surface HSPGs bearing long- or short-chain HS. (A) Cell lines expressing longer HS chains, such as NP-2 cells; (B) cell lines expressing shorter HS chains, such as U251MG cells.

to the cell surface (35) and that heparin induces the dimerization of NRP-1 (66), increasing ligand binding to NRP-1. These shorter HS chains might be able to produce receptor complexes (HTLV-1 Env-HS-NRP-1-GLUT1) more efficiently than that of longer HS chains by attracting the HTLV-1 particles to the target cell surface.

In this study, we observed that K4R cells expressing HSPGs aggregated in cultures, suggesting that the cell surface expression of HSPGs creates an environment to mediate the cell-to-cell transmission of HTLV-1 particles trapped on the surface of HTLV-1 producing cells. Intriguingly, the increased cell-cell adhesion of target cells induced by HSPGs does not augment membrane fusion with HTLV-1-producing cells. These results suggest that cell surface expression of HSPGs promotes the target cells to receive the HTLV-1 particles without cell fusion. In fact, it has been reported that HS chain expression decreases HTLV-1 Env-mediated syncytium formation (48). Because fused cells are likely to die *in vitro*, HSPGs may promote the survival of HTLV-1 infected cells.

In conclusion, our findings suggest that the interactions of HTLV-1 with SDCs bearing short HS chains containing heparin-like structures are important for efficient HTLV-1 infection. The combination of cell surface HS chain structure and the number of HS chains (the number of SDC core proteins) is one of the key factors affecting the cell tropism of HTLV-1. Future experiments are needed to correlate the differences in HS expression in target cells of HTLV-1, such as primary T cells and cells in other target tissues, with the cellular tropism of HTLV-1 *in vivo*. Nonetheless, the findings obtained in this study may provide the basis for developing effective therapies against HTLV-1 infection and an index for assessing the prognosis of disease associated with HTLV-1 infections.

#### ACKNOWLEDGMENTS

We thank M. A. Whitt for kindly supplying the VSV G-expressing pCAGGS/VSV-G plasmid and VSVΔG\*G; G. Nolan (Stanford University, Stanford, CA) and T. Kitamura (Institute of Medical Science, The University of Tokyo, Tokyo, Japan) for kindly providing the Phoenix-A and Plat-E retrovirus-packaging cell lines, respectively; Y. Tanaka (Division of Immunology, Faculty of Medicine, University of the Ryukyus, Okinawa, Japan) for kindly supplying the anti-HTLV-1 gp46 MAb, LAT-27; and S. Takase-Yoden (Faculty of Engineering and Graduate School of Engineering, Soka University, Tokyo, Japan), T. Miyazawa and P. Gee (Institute for Virus Research, Kyoto University, Kyoto, Japan), R. Watanabe (Department of Veterinary Medicine, Yamaguchi University, Yamaguchi, Japan), M. Saha (University Health Net-

work, Toronto, Canada), and J. Komano (AIDS Research Center National Institute of Infectious Diseases, Tokyo, Japan) for their suggestions and critical reading of the manuscript. We also thank M. Nakazawa and A. Nakamura (Graduate School of Medicine, Gunma University, Gunma, Japan) for their assistance with the statistical analyses.

This work was supported in part by grants-in-aid from the Japanese Society for the Promotion of Science, the Japan Health Sciences Foundation, and CREST.

#### REFERENCES

1. Akagi T, Shishido T, Murata K, Hanafusa H. 2000. v-Crk activates the phosphoinositide 3-kinase/AKT pathway in transformation. *Proc. Natl. Acad. Sci. U. S. A.* 97:7290–7295.
2. Bigner DD, et al. 1981. Heterogeneity of Genotypic and phenotypic characteristics of fifteen permanent cell lines derived from human gliomas. *J. Neuropathol. Exp. Neurol.* 40:201–229.
3. Coskun AK, Sutton RE. 2005. Expression of glucose transporter 1 confers susceptibility to human T-cell leukemia virus envelope-mediated fusion. *J. Virol.* 79:4150–4158.
4. David G, Bai XM, Van der Schueren B, Cassiman JJ, Van den Berghe H. 1992. Developmental changes in heparan sulfate expression: in situ detection with mAbs. *J. Cell Biol.* 119:961–975.
5. David G, et al. 1990. Molecular cloning of a phosphatidylinositol-anchored membrane heparan sulfate proteoglycan from human lung fibroblasts. *J. Cell Biol.* 111:3165–3176.
6. de Revel T, et al. 1993. In vitro infection of human macrophages with human T-cell leukemia virus type 1. *Blood* 81:1598–1606.
7. Esko JD. 1991. Genetic analysis of proteoglycan structure, function and metabolism. *Curr. Opin. Cell Biol.* 3:805–816.
8. Fischinger PJ, Peebles PT, Nomura S, Haapala DK. 1973. Isolation of RD-114-like oncornavirus from a cat cell line. *J. Virol.* 11:978–985.
9. Gallagher JT, Turnbull JE, Lyon M. 1990. Heparan sulphate proteoglycans. *Biochem. Soc. Trans.* 18:207–209.
10. Gessain A, et al. 1985. Antibodies to human T-lymphotropic virus type-I in patients with tropical spastic paraparesis. *Lancet* ii:407–410.
11. Gessain A, Boeri E, Yanagihara R, Gallo RC, Franchini G. 1993. Complete nucleotide sequence of a highly divergent human T-cell leukemia (lymphotropic) virus type I (HTLV-I) variant from Melanesia: genetic and phylogenetic relationship to HTLV-I strains from other geographical regions. *J. Virol.* 67:1015–1023.
12. Ghez D, Lepelletier Y, Jones KS, Pique C, Hermine O. 2010. Current concepts regarding the HTLV-1 receptor complex. *Retrovirology* 7:99.
13. Ghez D, et al. 2006. Neuropilin-1 is involved in human T-cell lymphotropic virus type 1 entry. *J. Virol.* 80:6844–6854.
14. Graham FL, et al. 1975. Studies on in vitro transformation by DNA and DNA fragments of human adenoviruses and simian virus 40. *Cold Spring Harbor Symp. Quant. Biol.* 39:637–650.
15. Haraguchi Y, et al. 1994. Detection of neutralizing antibodies against human T-cell leukemia virus type 1 using a cell-free infection system and polymerase chain reaction. *Int. J. Cancer* 59:416–421.

16. Hinuma Y, et al. 1981. Adult T-cell leukemia: antigen in an ATL cell line and detection of antibodies to the antigen in human sera. *Proc. Natl. Acad. Sci. U. S. A.* 78:6476–6480.
17. Ho DD, Rota TR, Hirsch MS. 1984. Infection of human endothelial cells by human T-lymphotropic virus type I. *Proc. Natl. Acad. Sci. U. S. A.* 81:7588–7590.
18. Hoshino H, et al. 1983. Establishment and characterization of 10 cell lines derived from patients with adult T-cell leukemia. *Proc. Natl. Acad. Sci. U. S. A.* 80:6061–6065.
19. Hoshino H, Nakamura T, Tanaka Y, Miyoshi I, Yanagihara R. 1993. Functional conservation of the neutralizing domains on the external envelope glycoprotein of cosmopolitan and melanesian strains of human T cell leukemia/lymphoma virus type I. *J. Infect. Dis.* 168:1368–1373.
20. Hoshino H, Shimoyama M, Miwa M, Sugimura T. 1983. Detection of lymphocytes producing a human retrovirus associated with adult T-cell leukemia by syncytia induction assay. *Proc. Natl. Acad. Sci. U. S. A.* 80:7337–7341.
21. Hoxie JA, Matthews DM, Cines DB. 1984. Infection of human endothelial cells by human T-cell leukemia virus type I. *Proc. Natl. Acad. Sci. U. S. A.* 81:7591–7595.
22. Igakura T, et al. 2003. Spread of HTLV-I between lymphocytes by virus-induced polarization of the cytoskeleton. *Science* 299:1713–1716.
23. Imberty A, Lortat-Jacob H, Perez S. 2007. Structural view of glycosaminoglycan-protein interactions. *Carbohydr. Res.* 342:430–439.
24. Jacobson S, Raine CS, Mingioli ES, McFarlin DE. 1988. Isolation of an HTLV-1-like retrovirus from patients with tropical spastic paraparesis. *Nature* 331:540–543.
25. Jastrebova N, Vanwildemeersch M, Lindahl U, Spillmann D. 2010. Heparan sulfate domain organization and sulfation modulate FGF-induced cell signaling. *J. Biol. Chem.* 285:26842–26851.
26. Jin Q, Agrawal L, VanHorn-Ali Z, Alkhatib G. 2006. Infection of CD4+ T lymphocytes by the human T cell leukemia virus type 1 is mediated by the glucose transporter GLUT-1: evidence using antibodies specific to the receptor's large extracellular domain. *Virology* 349:184–196.
27. Jones KS, Petrow-Sadowski C, Bertolette DC, Huang Y, Ruscetti FW. 2005. Heparan sulfate proteoglycans mediate attachment and entry of human T-cell leukemia virus type 1 virions into CD4+ T cells. *J. Virol.* 79:12692–12702.
28. Kent WJ. 2002. BLAT—the BLAST-like alignment tool. *Genome Res.* 12:656–664.
29. Kikukawa R, et al. 1986. Differential susceptibility to the acquired immunodeficiency syndrome retrovirus in cloned cells of human leukemic T-cell line Molt-4. *J. Virol.* 57:1159–1162.
30. Kim CW, Goldberger OA, Gallo RL, Bernfield M. 1994. Members of the syndecan family of heparan sulfate proteoglycans are expressed in distinct cell, tissue-, and development-specific patterns. *Mol. Biol. Cell* 5:797–805.
- 30a. Kinet S, et al. 2007. Isolated receptor binding domains of HTLV-1 and HTLV-2 envelopes bind Glut-1 on activated CD4+ and CD8+ T cells. *Retrovirology* 4:31.
31. Kinsella TM, Nolan GP. 1996. Episomal vectors rapidly and stably produce high-titer recombinant retrovirus. *Hum. Gene Ther.* 7:1405–1413.
32. Kitamura T, et al. 1995. Efficient screening of retroviral cDNA expression libraries. *Proc. Natl. Acad. Sci. U. S. A.* 92:9146–9150.
33. Kjellen L, Lindahl U. 1991. Proteoglycans: structures and interactions. *Annu. Rev. Biochem.* 60:443–475.
34. Koyanagi Y, et al. 1993. In vivo infection of human T-cell leukemia virus type I in non-T cells. *Virology* 196:25–33.
35. Lambert S, et al. 2009. HTLV-1 uses HSPG and neuropilin-1 for entry by molecular mimicry of VEGF165. *Blood* 113:5176–5185.
36. Langford JK, Stanley MJ, Cao D, Sanderson RD. 1998. Multiple heparan sulfate chains are required for optimal syndecan-1 function. *J. Biol. Chem.* 273:29965–29971.
37. Linker A, Hovsing P. 1984. Structural studies on heparin. Tetrasaccharides obtained by heparinase degradation. *Carbohydr. Res.* 127:75–94.
38. Majorovits E, et al. 2008. Human T-lymphotropic virus-1 visualized at the virological synapse by electron tomography. *PLoS One* 3:e2251.
39. Manel N, et al. 2003. The ubiquitous glucose transporter GLUT-1 is a receptor for HTLV. *Cell* 115:449–459.
40. McAllister RM, et al. 1971. Cultivation in vitro of cells derived from a human osteosarcoma. *Cancer* 27:397–402.
41. Miyoshi I, Kubonishi I, Yoshimoto S, Shiraiishi Y. 1981. A T-cell line derived from normal human cord leukocytes by co-culturing with human leukemic T-cells. *Gann* 72:978–981.
42. Morita S, Kojima T, Kitamura T. 2000. Plat-E: an efficient and stable system for transient packaging of retroviruses. *Gene Ther.* 7:1063–1066.
43. Nackaerts K, et al. 1997. Heparan sulfate proteoglycan expression in human lung-cancer cells. *Int. J. Cancer* 74:335–345.
44. Onishi M, et al. 1996. Applications of retrovirus-mediated expression cloning. *Exp. Hematol.* 24:324–329.
45. Osame M, et al. 1986. HTLV-I associated myelopathy, a new clinical entity. *Lancet* i:1031–1032.
46. Pais-Correia AM, et al. 2009. Biofilm-like extracellular viral assemblies mediate HTLV-1 cell-to-cell transmission at virological synapses. *Nat. Med.* 16:83–89.
47. Pear WS, Nolan GP, Scott ML, Baltimore D. 1993. Production of high-titer helper-free retroviruses by transient transfection. *Proc. Natl. Acad. Sci. U. S. A.* 90:8392–8396.
48. Pinon JD, et al. 2003. Human T-cell leukemia virus type 1 envelope glycoprotein gp46 interacts with cell surface heparan sulfate proteoglycans. *J. Virol.* 77:9922–9930.
49. Poesz BJ, et al. 1980. Detection and isolation of type C retrovirus particles from fresh and cultured lymphocytes of a patient with cutaneous T-cell lymphoma. *Proc. Natl. Acad. Sci. U. S. A.* 77:7415–7419.
50. Popovic M, et al. 1983. Isolation and transmission of human retrovirus (human T-cell leukemia virus). *Science* 219:856–859.
51. Richardson JH, Edwards AJ, Cruickshank JK, Rudge P, Dalglish AG. 1990. In vivo cellular tropism of human T-cell leukemia virus type 1. *J. Virol.* 64:5682–5687.
52. Saiki RK, et al. 1985. Enzymatic amplification of beta-globin genomic sequences and restriction site analysis for diagnosis of sickle cell anemia. *Science* 230:1350–1354.
53. Salahuddin SZ, et al. 1983. Restricted expression of human T-cell leukemia-lymphoma virus (HTLV) in transformed human umbilical cord blood lymphocytes. *Virology* 129:51–64.
54. Saphire AC, Bobardt MD, Zhang Z, David G, Gallay PA. 2001. Syndecans serve as attachment receptors for human immunodeficiency virus type 1 on macrophages. *J. Virol.* 75:9187–9200.
55. Schultz RM, Woods WA, Chirigos MA. 1975. Detection in colorectal carcinoma patients of antibody cytotoxic to established cell strains derived from carcinoma of the human colon and rectum. *Int. J. Cancer* 16:16–23.
56. Sebestyen A, et al. 2000. Syndecan-1-dependent homotypic cell adhesion in HT58 lymphoma cells. *Tumour Biol.* 21:349–357.
57. Shafti-Keramat S, et al. 2003. Different heparan sulfate proteoglycans serve as cellular receptors for human papillomaviruses. *J. Virol.* 77:13125–13135.
58. Soda Y, et al. 1999. Establishment of a new system for determination of coreceptor usages of HIV based on the human glioma NP-2 cell line. *Biochem. Biophys. Res. Commun.* 258:313–321.
59. Sommerfelt MA, Weiss RA. 1990. Receptor interference groups of 20 retroviruses plating on human cells. *Virology* 176:58–69.
60. Stanley MJ, Liebersbach BF, Liu W, Anhalt DJ, Sanderson RD. 1995. Heparan sulfate-mediated cell aggregation. Syndecans-1 and -4 mediate intercellular adhesion following their transfection into human B lymphoid cells. *J. Biol. Chem.* 270:5077–5083.
61. Staples GO, Shi X, Zaia J. 2010. Extended N-sulfated domains reside at the nonreducing end of heparan sulfate chains. *J. Biol. Chem.* 285:18336–18343.
62. Takada A, et al. 1997. A system for functional analysis of Ebola virus glycoprotein. *Proc. Natl. Acad. Sci. U. S. A.* 94:14764–14769.
63. Tanaka Y, Zeng L, Shiraki H, Shida H, Tozawa H. 1991. Identification of a neutralization epitope on the envelope gp46 antigen of human T cell leukemia virus type I and induction of neutralizing antibody by peptide immunization. *J. Immunol.* 147:354–360.
64. Turnbull J, Powell A, Guimond S. 2001. Heparan sulfate: decoding a dynamic multifunctional cell regulator. *Trends Cell Biol.* 11:75–82.
65. van den Born J, et al. 2005. Novel heparan sulfate structures revealed by monoclonal antibodies. *J. Biol. Chem.* 280:20516–20523.
66. Vander Kooi CW, et al. 2007. Structural basis for ligand and heparin binding to neuropilin B domains. *Proc. Natl. Acad. Sci. U. S. A.* 104:6152–6157.
67. Van Der Maaten MJ, Miller JM. 1975. Replication of bovine leukemia virus in monolayer cell cultures. *Bibl. Haematol.* 1975:360–362.
68. Wu ZL, Lech M. 2005. Characterizing the non-reducing end structure of heparan sulfate. *J. Biol. Chem.* 280:33749–33755.
69. Yamada M, Watabe K, Saida T, Kim SU. 1991. Increased susceptibility of human fetal astrocytes to human T-lymphotropic virus type I in culture. *J. Neuropathol. Exp. Neurol.* 50:97–107.